DESIGN AND RADIATION CHARACTERISTICS OF OPTICAL ANTENNAS

ULVİHAN UĞUR DÜNDAR

JUNE 2018

DESING AND RADIATION CHARACTERISTICS OF OPTICAL ANTENNAS

A THESIS SUBMITTED TO
THE GRADUATE SCHOOL OF NATURAL AND APPLIED SCIENCES OF
ÇANKAYA UNIVERSITY

BY
ULVİHAN UĞUR DÜNDAR

IN PARTIAL FULFILLMENT OF THE REQUIREMENTS FOR THE DEGREE OF
MASTER OF SCIENCE
IN
THE DEPARTMENT OF
ELECTRONIC AND COMMUNICATION ENGINEERING

JUNE 2018

Title of the Thesis: **Design and Radiation Characteristics of Optical Antennas.**

Submitted by **Ulvihan Uğur DÜNDAR**

Approval of the Graduate School of Natural and Applied Sciences, Çankaya University.

Prof. Dr. Can ÇOĞUN
Director

I certify that this thesis satisfies all the requirements as a thesis for the degree of Master of Science.

Dr. Özgür ERGÜL
Head of Department

This is to certify that we have read this thesis and that in our opinion it is fully adequate, in scope and quality, as a thesis for the degree of Master of Science.

Prof. Dr. Yusuf Ziya UMUL
Supervisor

Examination Date: 26.06.2018

Examining Committee Members

Prof. Dr. Yusuf Ziya UMUL	Çankaya University	
Doç. Dr. Nursel AKÇAM	Gazi University	
Doç. Dr. Hüsnü Deniz BAŞDEMİR	Çankaya University	

STATEMENT OF NON-PLAGIARISM PAGE

I hereby declare that all information in this document has been obtained and presented in accordance with academic rules and ethical conduct. I also declare that, as required by these rules and conduct, I have fully cited and referenced all material and results that are not original to this work.

Name, Last Name	:	Ulvihan Uğur DÜNDAR
Signature	:	
Date	:	26.06.2018

ABSTRACT

DESIGN AND RADIATION CHARACTERISTICS OF OPTICAL ANTENNAS

DÜNDAR, Ulvihan Uğur
M.Sc., Department of Electronic and Communication Engineering
Supervisor: Prof. Dr. Yusuf Ziya UMUL
June 2018, 70 pages

In this thesis, the design of the optical antennas and their radiation properties was investigated. Firstly, the principle of operation of optical antennas, the relation between structure and light and matter, design of various optical antenna designs, calculation of radiation fields was made. These radiation fields were calculated in the analytically using the physical optics integral. These calculations were made for each optical antenna and radiation fields are observed. The MATLAB program was used to examine the radiation fields and calculated the physical optic integral. In this way, the various optical antennas designed in that their performance and their radiating properties were shown and the corresponding drawings were included in this thesis.

Keywords: Optical Antenna, Physical Optic, Radiation Pattern.

ÖZ

OPTİK ANTENLERİN TASARIMI VE IŞIMA ÖZELLİKLERİ

DÜNDAR, Ulvihan Uğur
Yüksek Lisans, Elektronik ve Haberleşme Mühendisliği Anabilim Dalı
Tez Yöneticisi: Prof. Dr. Yusuf Ziya UMUL
Haziran 2018, 70 sayfa

Bu tezde optik antenlerin tasarımları ve ışıma özellikleri incelenmiştir. Öncelikle optik antenlerin çalışması prensibi, yapıları ve ışık ile madde arasındaki ilişki incelenip, çeşitli optik anten tasarımları tasarlanarak, ışıma alanlarının hesabı yapılmıştır. Bu ışıma alanları fiziksel optik integrali kullanılarak, analitik olarak hesaplanmıştır. Her bir optik anten için hesaplama yapılıp, ışıma alanları gözlemlenmiştir. Işıma alanlarının incelenmesi ve fiziksel optik integralinin hesaplanması için MATLAB programı kullanılmıştır. Bu yolla, tasarlanan çeşitli optik antenlerin, performansı ve ışıma özellikleri çıkarılmış, ilgili çizimler bu tezde yer bulmaktadır.

Anahtar Kelimeler: Optik Anten, Fiziksel Optik, Işıma Diyagramı.

ACKNOWLEDGEMENTS

I would like to express my sincere gratitude to Prof. Dr. Yusuf Ziya UMUL for his supervision, special guidance, suggestions, and encouragement through the development of this thesis.

It is a pleasure to express my special thanks to my family for their valuable support.

TABLE OF CONTENTS

LIST OF FIGURES

FIGURES

LIST OF TABLES

TABLES

LIST OF ABBREVIATIONS

BGE	Band Gap Energy
BTA	Bow Tie Antenna
CB	Conduction Band
DA	Dipole Antenna
DT	Drude Theory
EUV	Extreme Ultraviolet
EBL	Electron Beam Lithography
FDTD	Finite Difference Time Domain
FSO	Free Space Optic
FEM	Finite Element Method
GO	Geometrical Optics
IB	Ion Beam
KE	Kinetic Energy
LA	Lithographic Antenna
LED	Light Emitting Diode
PE	Photoelectric Effect
PO	Physical Optics
OA	Optical Antenna
OCA	Optical Circular Antenna
ODA	Optical Dipole Antenna
OTA	Optical Triangle Antenna
OQCA	Optical Quarter Circular Antenna
SERS	Surface Enhanced Raman Scattering
SNOM	Scanning Near-Field Optical Microscopy
STM	Surface Tunneling Microscopy

WF	Work Function
VB	Valence Band
VLC	Visible Light Communication

CHAPTER 1

INTRODUCTION

1.1 Antenna Theory

An antenna is the most important device for communication and other systems because signals (electromagnetic waves) are transmitted through the device which is defined in IEEE standard 145 which was published in 1983. Antenna means radiating or receiving radio waves (electromagnetic waves) [1]. Components of electromagnetic wave consist of electric and magnetic field. Electric field means force per load, magnetic field means time dependent Lorentz force of moving load. Antennas enable electromagnetic waves to travel from point to point in free space for communication and other applications.

Theory of antenna was first studied by James Clerk Maxwell who invented the relations known as Maxwell Equations [2]. First antenna that was designed by Marconi in 1906, used 70 meters wood towers. Its power was 50 kW and had a wavelength of 2000 – 10000 m [3]. Its operation frequency was between 3-15 kHz. Nowadays, technologies of antenna are developing faster year to year and antenna dimensions are smaller, their operation frequencies and data ranges are higher. Operation frequency range of these antennas are 1-40 GHz by area of use. Application areas of antenna are Global System for Mobile Communication (GSM), Television (TV), Radio, Radar, Mobile Phone (MP). Small dimension antennas are generally used in Mobile Phone, Bluetooth and ZigBee. High frequency antennas are used in Radar, Television, GSM, Radio towers.

1.2 Optical Antenna Theory

Many researchers have studied antennas, especially optical antennas because traditional antennas have some problems which are narrow bandwidth [4], more diffraction and resolution. Optical Antennas (OA) reduced these kind of problems [5]. In recent years, optical systems are dependent on bandwidth of electronic systems but this problem is overcome through nanotechnology. Traditional antennas use electromagnetic field which are microwave and radio for modulation. OAs are used in lenses, mirrors [6]. Therefore, required areas of using OA are detection and imaging such as spectroscopy, short range communication radiation thermometer, night vision.

In literature, there are a lot of problems about traditional antennas. These problems are communication, narrow bandwidth, more diffraction and resolution, so OAs are needed. They are converting incident laser wave (incident light) on antenna surface to electromagnetic field with using lens and structure of small dimension. OAs were firstly described in [7] by Synge who told Einstein about microscopic method which defines scattered electromagnetic field as incident tiny particles from a laser source. In 1928, Edward Hutchinson Synge told about the microscopic method to Einstein through [8] and Einstein started to study this method in [9]. Microscopy method observes the optical frequency on antenna surface. Optical frequencies are high frequencies that have small wavelengths which are between 100-118 nm. Other sensing technique of these particles are Surface Enhanced Raman Scattering (SERS) and Surface Tunneling Microscopy (STM).

OAs have small dimensions (nanometer, nm) so they can’t be measured with traditional antenna measurement techniques. Radiating electromagnetic field is measured by the surface current on antenna. The most commonly used measurement device in literature is photodetector which calculates the radiation of electromagnetic field. Specifications of optical antennas are small dimension (140-200 nm) and wavelength (100-118 nm), high frequency (10-100 PHz) [7].

Fundamental of operation of optical antenna is the interaction between photons and electrons which occurs when incident photons from a light source collide on the surface of antenna. After the interaction between them, energy level of the electron rises and the electron leaves this energy level, and moves on the surface of the antenna as shown in Figure 1 [7].

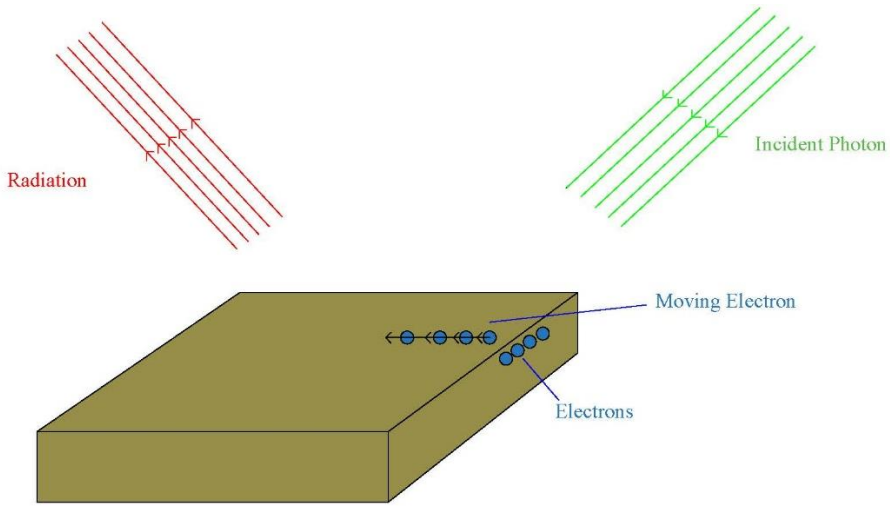

Figure 1 Operation of optical antenna [7]

After this case, current occurs on the surface of the antenna causing the presence of a radiation field which is sensed by photodetectors. In Ch. 3 will give details about this event. Block diagram of Optical Antenna is shown in Figure 2 [7].

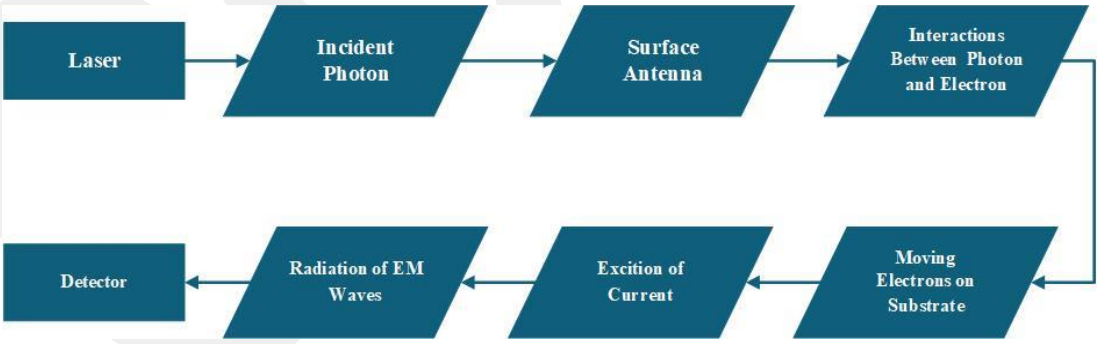

Figure 2 Block diagram of optical antenna [7]

In literature, several groups from Stanford University and University of Central Florida [10] have studied different techniques, methods and experimental setups about on OAs. There are several designs, researches and experiments on OAs such as Bow

Tie Antenna (BTA) and Dipole Antenna (DA). In first experiment [11], near-field optical probe is used to design a BTA which had lower diffraction limit and more transmission efficiency. Experimental setup and BTA are shown in Figure 3.

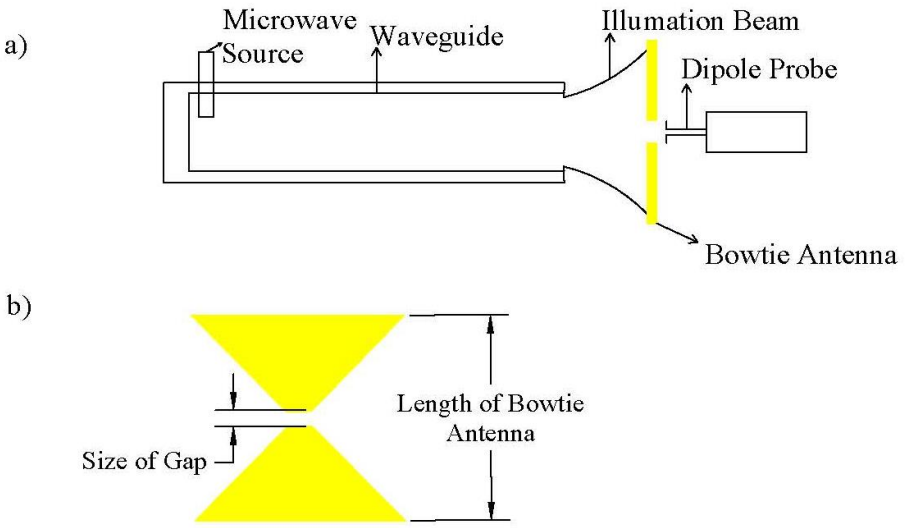

Figure 3 a) Experimental setup of BTA, b) Bow tie antenna

Design parameters of experimental setup were the microwave source, the waveguide, the illumination beam, the dipole probe and the size of the gap, BTA, the total length. Feeding point of BTA was microwave source which had frequency of 2.20 GHz, wavelength of 13.6 cm. Electromagnetic wave travelled inside waveguide and illumination beam. Total length of BTA (L) was 36 cm (2.6λ). BTA was mounted between illumination beam and dipole probe which has a total length of arms of 0.7 cm (~λ/20). Result of this experiment setup was theoretically verified and this provided a basis of BTA for near-field optics. In second experiment, Extreme UltraViolet (EUV) wavelength of laser in BTA was observed in [12]. BTA was structured as arrays that is shown in Figure 4. Experimental setup had Ti: sapphire oscillator which is a laser oscillator that has pulse duration of <10 fs and a pulse energy of till 5 nJ centered in 820 nm. Lens was placed on focal position that has spot size range from 20.6x13.8 to 8.2x 5.6 μm. Dimensions of BTA were from 140 to 200 nm in length and 50nm in thickness.

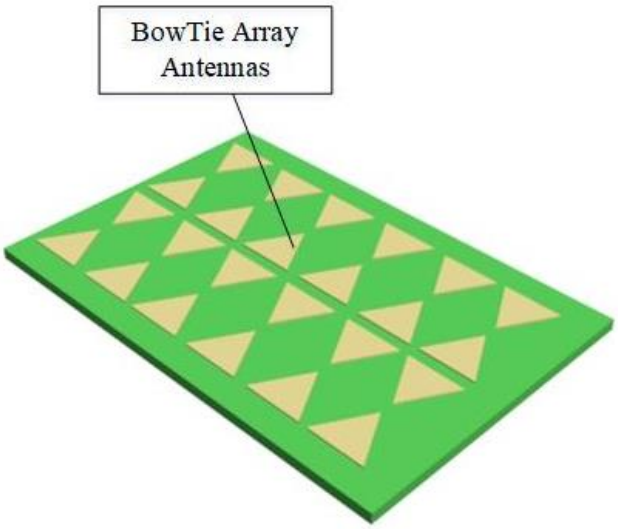

Figure 4 Array structure of BTA

The results of analysis were measured radiation wavelength of 118 nm, frequency of 2.5 PHz and more plasmonic field occurrence over surface of BTA. In the third experiment on BTA, EUV light and harmonic generation wavelength of femtosecond laser was studied in [13]. Design parameters of BTA were height of 175 nm, gap of 20 nm, thickness of 50 nm, angle of 30^0. The experiment setup also included an incident pulse laser with a bandwidth of 100 nm and a carrier wavelength of 800 nm. BTA was defined by Debye Model (DM). Results of the experiment successfully verified 20 nm gap, output power peak of 100 kW and pulse intensity of 10^{11} Wcm^{-2} from generation of EUV. In fourth experiment, different distances of gap size, resonant wavelength and shape of BTA were investigated in [14]. The method of Finite Difference Time Domain (FDTD) was applied to observe the current on BTA. Design of BTA were length of 88 nm, thickness of 24 nm, gap size from 16 to 500 nm and triangle apex has radius of curvature at 12 nm. Structure of BTA was Gold (Au). At the end of the experiment, resonant wavelength was observed. Result of experiment was consistent with theoretical calculations. Especially near-field and optical probe provided low diffraction limit. Fifth experiment in [15] used the same method as previous experiment on BTA. In the experiment, two excited photons were used to improve local intensity factors for surface on BTAs. Local intensity was defined in a specific area. Experimental setup has Tİ: sapphire laser with a pulse duration of 120 fs and

wavelength of 830 nm. Design of BTA in this experiment was based on gold BTA which had a length of 1.56 μm, thickness of 60 nm [16] and another BTA with length of 75 nm, thickness of 20 nm [17]. The end of experiment resulted in like previous experiment. Same theory and calculation was observed in FDTD simulation.

Seen in the literature, several experiments and simulations were made about DAs. First the experiment, Lithographic Antenna (LA) demonstrated in [18] efficient with using mid-infrared frequency. Shape of LA was designed in the dipole antenna (DA) which was total length 6.7 μm. Expected of the experiment was thermal and photoelectric effect. The experiment setup had been consisted of He-Ne laser copped at operation frequency 400 Hz and focused on focal length of 40 mm, an aperture diameter of 22 mm. The result of the experiment was observed on wavelength of incident wave smaller than wavelength of receive wave. Second the experiment, observation field intensity on DA with range infrared wavelength was studied in [19]. Applied method, simulation, model is used to on Finite Element Method (FEM), software HFSS and Drude Theory (DT). Structure of DA was separated on gold. Design parameters of DA were arm's length of 250 nm, width of 100 nm, thickness of 30 nm and feed gap of 30 nm. Feed gap, width, length of DA was changed dimensions that is order 20-60 nm, 20-90 nm, raised steps 40nm between 230-530 nm. Polarization angle of surface on antenna was increased between 0^0 to 90^0 by steps 15^0. Increased feed gap and width were reduced on intensity field but increased length of DA was raised on intensity field over DA. Intensity field was maximum 0^0 on antenna. Depending on geometry of DA was changed intensity field. In third experiment was investigated in [20] power, radiation, latency, noise different resonant wavelengths on DA with using FDTD method for germanium photodetector and was applied near-field technique. Wide, thick, long of DA is in order of 50 nm, 50 nm, 160 nm. Depending on resonant wavelength of DA is changed measurement intensity field with using germanium photodetector.

In recent years, in literature studies about optical antennas had been done between in 2016-2018. These were experimental setups, simulations for optical antennas. In first was studied in [21] the simulation for dipole antenna. Design of dipole antenna

had been length of 1.1 μm, width of 160 nm and thick of 60 nm with using gold material. The dipole antenna was designed as a waveguide which observed on interaction electrons and photons inside in the waveguide. Wavelength of source was 850 nm. Using the COMSOL program, the design of the dipole antenna was investigated. The result of the simulation was observed on different the wavelength of sources in the propagation. For example, observed on the propagation wavelength of 10 μm and the wavelength of source was 900 nm. In second was studied in [22] experimental setup for dipole antenna. Design parameters of dipole antenna were different widths and constant length with using gold material. Widths of dipole antenna were 30 nm, 60 nm, and 90 nm. Length of dipole antenna was 655 nm. The result of the experiment was investigated in radiation frequency from different design of dipole antenna. In third was studied in [23] experimental setup with using different materials and epsilons (ε). These materials were Ga:ZnO, Al:ZnO, and ZnO. Lengths of dipole antenna from different materials were 600 nm for Ga:ZnO, 400 nm for Al:ZnO, and 800 nm for ZnO. Thick of dipole antenna from different materials was 1.4 μm for Ga:ZnO and Al:ZnO. The result of the experiment was demonstrated in radiation patterns for these materials and observed on radiation patterns from different epsilons. In fourth was studied in [24] the simulation for different designs of optical antenna. These designs of optical antenna were slot dipole antenna, slot crossed dipole antenna, and slot bow-tie antenna. Designs parameters of slot dipole antenna were contained on length of 0.84 μm, width of 4.8 μm, and feed point width of 0.6 μm. Designs parameters of slot crossed dipole antenna were contained on length of 5.175 μm, width of 0.345 μm. Designs parameters of slot bow-tie antenna were contained on length of 3.335 μm, width of 2.224 μm, and feed point width of 0.445 μm. Using material of these antennas was gold. The result of the simulations observed in the radiation frequencies and gains in these antennas. In fifth was studied in [25] the simulation for hexagonal ring optical antenna. Using simulation program was CST microwave studio. Design parameters of hexagonal ring optical antenna were inner radi at 580 nm and 765 nm, width of ring at 115 nm. The result of the simulations observed on radiation characteristics from different radius of curvature and radiation frequencies.

As a mentioned above, researches are worked on experimental setup, simulations that is researched on dipole and bow-tie antenna, there is no design depending on analytic calculation. Because of our aim of in thesis will analytic calculation, different on type of OAs.

1.3 Organization of Thesis

This organization of thesis consists of six chapters. All analysis of analytic and calculations are studied original design of different type of optical antenna and observed on radiation pattern. End of this thesis shows in more efficient and new technology which type of antenna.

Chapter 1 is an introduction to the history traditional antenna and optical antenna, searched about literature studied on optical antennas and objectives of this thesis.

Chapter 2 includes a fundamental of light – matter which gives about information of interaction of light – matter, photovoltaic effect, band gap, fermi energy, valance and conduction band.

Chapter 3, detailed about operation, structure, production technique of optical antenna.

Chapter 4, designed and calculated of optical antenna which types of shape antenna.

Chapter 5, observed in radiation pattern of different shape of optical antenna with using MATLAB program. Result of this chapter 5 compared on types of optical antenna.

Chapter 6 has the conclusion part.

CHAPTER 2

FUNDAMENTALS OF LIGHT – MATTER INTERACTIONS

2.1 Interaction of Light with Matter

Nowadays, light is playing very important role in our life and in technology because is being used in a lot of application areas which are Fiber Optic, Visible Light Communication (VLC), Free Space Optic (FSO), Light Emitting Diode (LED), Optic Antenna, Nanolithography Technology, X-ray devices, cutting operation. Light contains in the small particles which are photons [26]. In the Quantum Theory is defined in photon that interact on matter's electron that radiate electromagnetic wave. Specifications of photons have zero mass and speed of light. Actually, light described in [27] that was an electromagnetic wave which wavelength between 10^{-16} - 10^{8} meter, frequency between 10^{24} - 10^{0} Hz. Electromagnetic spectrum is shown as in Figure 5.

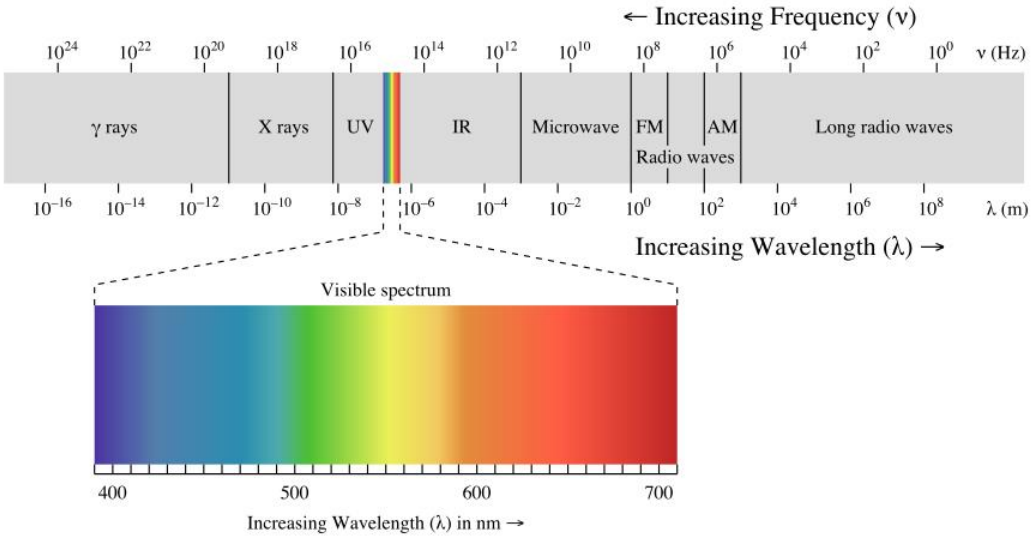

Figure 5 Electromagnetic spectrum [28]

Electromagnetic spectrum is applied in the various application technologies with different frequencies and wavelengths. There are Gama Rays, X-Ray, UV, Visible, Infrared, Microwave, Radio and Long Radio Waves.

Matter is described that have mass and any volume an object that is consist of atoms. Status of matter are types of solid, liquid and gas. Changed frequency and wavelength of electromagnetic waves impact different reaction radiation waves over matter. In this section will give about in atom models. There are atom models in the literature such as Thomson's, Rutherford's and Bohr's.

Thomson's atom model was firstly proposed in 1904 by J.J. Thomson [29]. This model was described in [30], because of electrons and positive loads had been pushed-pulled each other, negative load electrons were located in the spherical around the positive loads in atom. This model name would be Plum Pudding atom model. According to Plum Pudding model, when atoms have low energy, electrons are fixed their energy level. If atom has excited, electrons are oscillated around the energy level. Because of accelerated loads propagated on electromagnetic radiation like oscillation electrons, this event was supported in the Thomson's atom model.

Rutherford had studied on Thomson's atom model and had understood this atom model. Therefore, he established in [31] an experiment using gold-foil in 1911. Experimental setup consisted of a layer gold-foil 40 μm, α and β particles. This experiment was observed in that incident particle (α) has ν velocity which follows hyperbola path but went different ν' velocity far away from atom. This event's name was Rutherford's atom model. Rutherford's atom model became more valid than Thomson's atom model.

Niels Bohr was studied on [32-33-34] a new atom model in 1913 that was Bohr's atom model. Definition of its were given in 4 suggestions by Bohr. These suggestions are;

1- Under Coulomb attraction an electron moves around in an atom in circular orbit.

2- Instead of infinity of orbits are changed an orbit representation angular momentum and Planck constant.
3- Energy of electron is constant on location an orbit.
4- If Energy level of electron is changed, frequency of emitted radiation is found below equation.

$$f = \frac{(E_2 - E_1)}{h} \tag{2.1}$$

where f is the frequency of emitted radiation, E_1 and E_2 are energy of orbit levels, h is Planck constant.

According to these suggestion, understood relation between electron to atom and relation between electron to photon. Bohr's atom model was used Hydrogen atom which has one proton which is shown as in Figure 6.

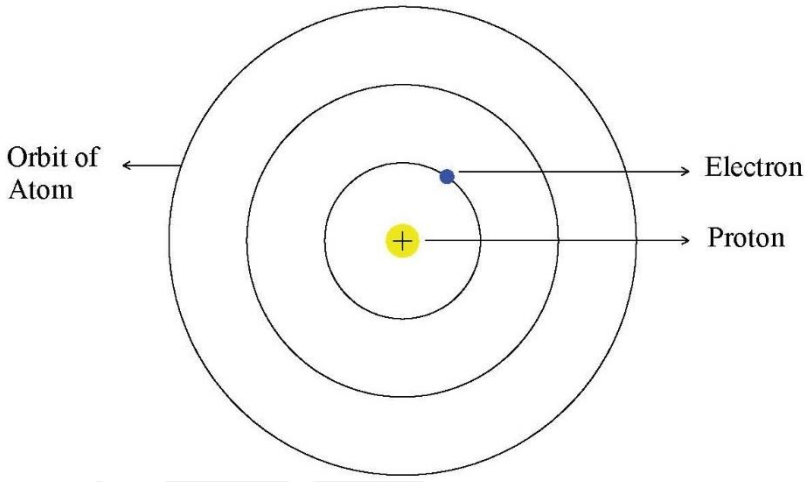

Figure 6 Hydrogen atom

Description of Bohr's atom model is shown as in Figure 7 that incident photon collisions electron in the orbit and transfers photon energy to electron. After this event, electron goes up to the top orbit. When electron comes back normal orbit, observes emission of the electron energy.

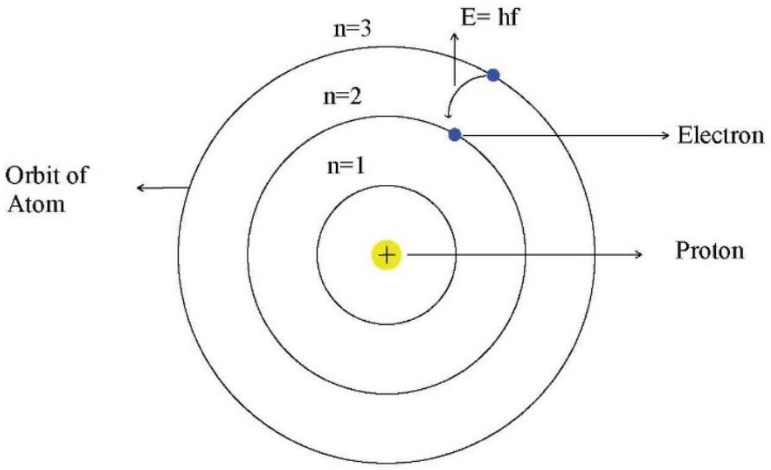

Figure 7 Bohr's atom model

According to in atoms from the periodic table, observes different emission of energy. Interaction of light – matter depend on atom models, have various interactions.

2.2 Photoelectric Effect (PE)

Nature of light and matter based on the quantum mechanics. Photoelectric Effect (PE) was found in [35] 1887 by Heinrich Hertz who established in the experimental setup. The end of experiment was observed 4 results. First result, when on metals were scattered, emitted electrons. Second result, electrons emission depended on from the wavelength of incident light and the frequency of incident light was greater than threshold frequency of metals. Third result, the magnetic of surface current depended on the intensity of light. Fourth result, the energy of emit electron depended on linearly with the frequency of incident light. Thanks to the experiment, based on fundamental of PE. Max Planck was described in [36] electromagnetic radiation which consisted of energy packets and transported in 1901 by them. In 1905, Albert Einstein researched in [37] question theory of light that proposed PE. According to Albert Einstein, energy of incident photon collided in electrons on surface metal. Electron emitted in energy of photon and moved in case of Kinetic Energy (KE) to far away from electron in atom. Energy of incident photon described as

$$E_p = hf_p \tag{2.2}$$

where E_p and f_p are energy of incident photon, frequency of incident photon. Kinetic energy of electron can be written as

$$K_e = E_p - w \tag{2.3}$$

Used Eq. (2.2) in Eq. (2.3) can be written as

$$K_e = \left(hf_p\right) - w \tag{2.4}$$

where K_e and w are kinetic energy of electron, work function. Work Function (WF) means [38] that is energy of required for moving away electron in atom. Table 1 shows in [39] WF values for Silicon, Gold, Copper, Aluminum.

Table 1 Work Function (WF)

Material	**Work Function (eV)**
Silicon	4.85
Gold	5.10
Copper	4.66
Aluminum	4.28

If energy of incident photon has no enough or energy of WF is greater than energy of incident photon, electron doesn't leave in orbit of electron so energy of WF is smaller than energy of incident photon. Eq. (2.4) defined in the K_e of electron on the surface metal. K_e of electron was described in other mathematical as

$$K_e = \frac{1}{2}mv_e^2 \tag{2.5}$$

where m and v_e are mass of electron, velocity of electron. Known of K_e of electron is founded velocity of electron by Eq. (2.5). Frequency of electron (f_e) can be written as

$$f_e = \frac{mv_e^2}{2h} \tag{2.6}$$

In this Eq. (2.6), Frequency of electron is found electromagnetic spectrum range.

Application of PE are medical applications [40], led emitting diodes [41], laser [42], nanoelectronics devices [43]. Application of medical for PE had developed in [40] optical gain from nanocrystal quantum dots. In this research was observed on simulation of quantum dots emission in the nanoparticles. Radius of quantum dots

were dimension 7 nm from in the narrowband. Quantum efficiency was %50 in the room temperature with visible spectrum. In result of this research was threshold behavior from quantum dots.

For led emitting diodes, the new materials were developed in [41] this experiment such as silicon especially. The experiment is used CdSe material. Researchers observed in the advantage of the developments which contained in the preparation and the characterization of gap semiconductors. The material was exposed a light source which was X-ray range. Hence, the result of experiment was based on the structure of materials which had been different photo-emission and realized on many advantageous which were low operating voltage and high efficiencies.

For laser, established in [42] the experimental setup which features of laser were argon-ion materials, wavelength 476.1 nm, power 0.1 mW and were used the CdSe material. In this experiment were observed on the different wavelengths of the laser which were optical properties, photoluminescence efficiency, transmission electron microscopy and photovoltaic devices. Optical density was much value from low wavelengths for optical properties and photoluminescence efficiency was found in the range %21-24. For transmission electron microscopy observed on exciton and transfer in the CdSe material surface. For photovoltaic devices found graph of current and voltage in the CdSe material specifications.

For nanoelectronics devices, established in [43] the experimental setup. This research methods were higher-resolution transmission electron microscopy and X-ray diffraction. Thanks to the experimental realized on band gap engineering for optical properties. In the experimental setup was contained in the shape of nanowires to use $CdS_{1-x}Se_x$ materials. The length of nanowires was uniform 10 μm. Results of the experiment was observed on fundamentals of band gap engineering, emission and refractivity in optical properties, carrier mobility and threshold voltage in the electrical properties. Also, under different photon energies in nanowires was shown on absorbance rate on the material.

2.3 Energy Bands of Semiconductor

In recent years, electronics is technology of regulation the stream of electrons however photonics is technology of regulation the stream of photons. Hence, electronics and photonics have been combined in semiconductor optoelectronic and electronic devices. The semiconductors are absorbed and emitted the through photons in the undergoing optoelectronic and electronic device in different energy levels. Operation of all semiconductor optoelectronic devices includes two processes. The first process is the absorption of a photon can generate an electron-hole pair. The result of charge carriers from absorption can interchange the electrical properties of the material. The effect is photoconductivity. The second process is the combination between an electron and a hole can observe in the emission of a photon. This process is like the operation of semiconductors as light source. Radiative electron-hole combination is the occurring process of light generation in the light emitting diode. Thus, interaction of semiconductor and electrons consists of these two processes [44].

Semiconductors are used on applications of electronic which are designed structure of capacitor, resistor, transistor, electronic chips and technologies of optic are used application areas which are designed lens, fiber optic cable, laser. Semiconductors are provided on electric resistivity for electronic devices and are interacted on light for optic technologies. According to the electronic devices and optic technologies are used popular Silicon, Gold, Copper, Aluminum. There materials have different energy gaps [37] which are called Band Gap Energy (BGE). Band Gap Energy of different materials are shown as Table 2.

Table 2 Band Gap Energy

Material	Band Gap Energy (eV)
Silicon	1.17
Gold	1.52
Copper	1.35
Aluminum	1.26

Band Gap Energy means that electrons are require energy between valence band and conduction band for passing. Valence Band (VB) has highest energy of electrons but Conduction Band (CB) has lowest energy of electrons and has widely empty of electron [37].

Figure 8 Conduction and valence band

Valence and Conduction Bands are shown in Figure 8. When interaction of photon and electron occurs inside of VB, energy of electron is raised. If energy of electron is greater than Band Gap Energy, electron is transported and is moved inside of CB. Surface current is observed on CB. If energy of electron is highest from range of CB, electron leaves on surface in CB.

CHAPTER 3

OPTICAL ANTENNA

3.1 Operation of Optical Antenna

In literature, many researches had studied about operation of OAs. In these investigations included in many experiments and simulations. It observed on [45] detection of optical radiation and frequency from OAs. In these observations were setted several the experimental setups and were designed different shapes for OAs. Parts of the experimental setup were used lasers, lenses, mirrors, fibers, photodetectors to observe on propagation of optical radiation and frequency which means high frequency between 10-100 PHz [7] and small dimension between 140-200 nm [12]. In the first experiment was observed in [46] the optical frequency from optical patch antenna. Design parameter of the optical patch antenna were radius 600 nm, thickness 20 nm. The observation point was 20 nm from optical patch antenna. Incident photon had 5 wavelengths. Result of observation was gotten on 2 peaks in the optical frequency. In the second experiment was investigated in [47] asymmetric nano-optical antenna. Operation of as asymmetric nano-optical antenna was distribution of the scattered photon momentum. Asymmetric nano-optical antenna was feeded with laser that observed on radiation from scattered photon momentum. In the third experiment was designed in [48] the nanowire optical antenna. Radiation of the nanowire optical antenna was detected on emitting photon response. These experiments are feed on these optical antennas with the laser.

Systems of OA has different techniques and designs in literature. According to in the literature, are mentioned operation of OAs that are feeded from lasers which has wavelength between 820-830 nm [12]. Feeding of OAs is focused with lens that

photons come from the laser focusing on the OA surface. Incident photons are collided inside of OA with the electrons. The end of collision is interaction between electrons and photons that electrons are moved on the OA surface which is occurred on the surface current. The resulting current causes the photon to be radiated from the antenna surface. Collection of photons is made with the photodetector and is observed on radiation of OA [7].

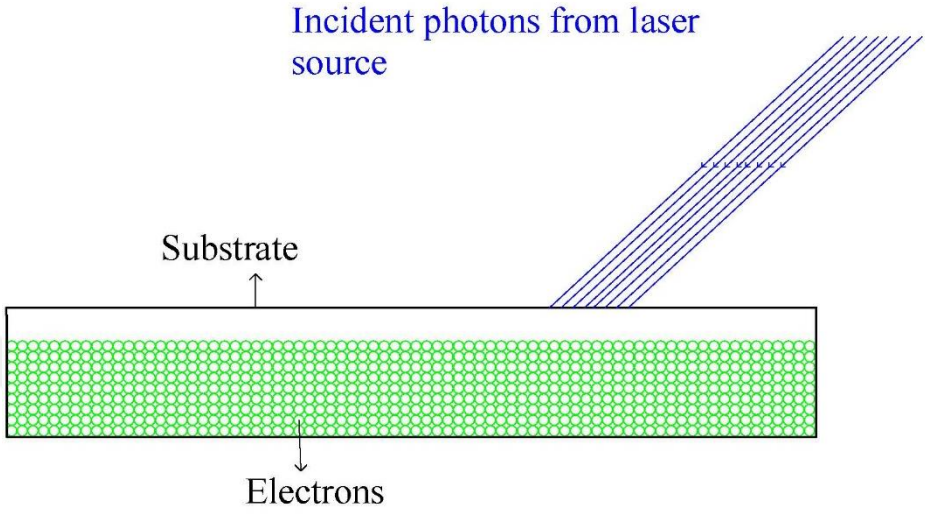

Figure 9 Incident photons from laser source

Figure 9 is shown incident photos from laser source comes electrons in OA surface. Feeding of OA is focused on surface through lens. Frequency of laser is between 36.1-36.5 PHz and wavelength between 820-830 nm.

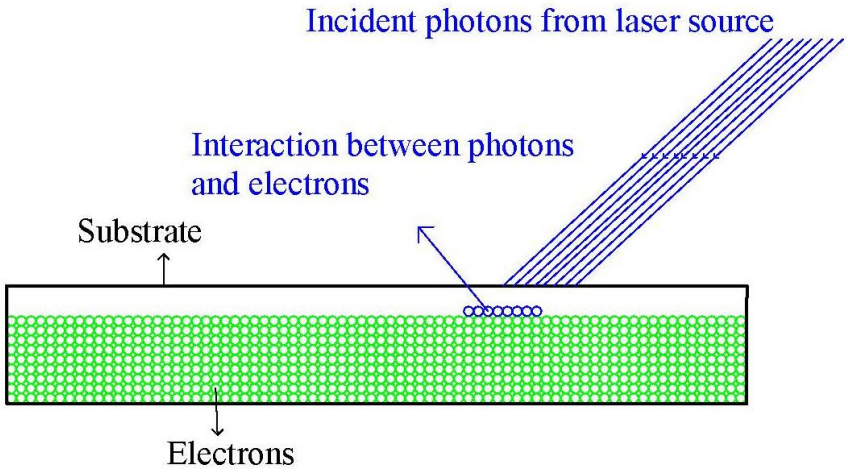

Figure 10 Interaction between photons and electrons

Figure 10 is shown interactions between photons and electrons observes in OA. Rising energy of electrons are moved on inside substrate and occurred current over surface OA.

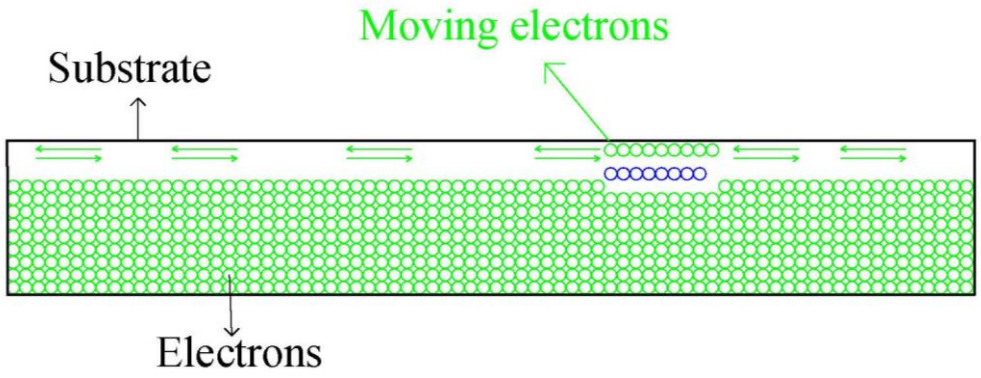

Figure 11 Electron moving in OA

Figure 11 shows electrons moves in OA surface which observes surface current. Electrons moved on along the boundary of OA.

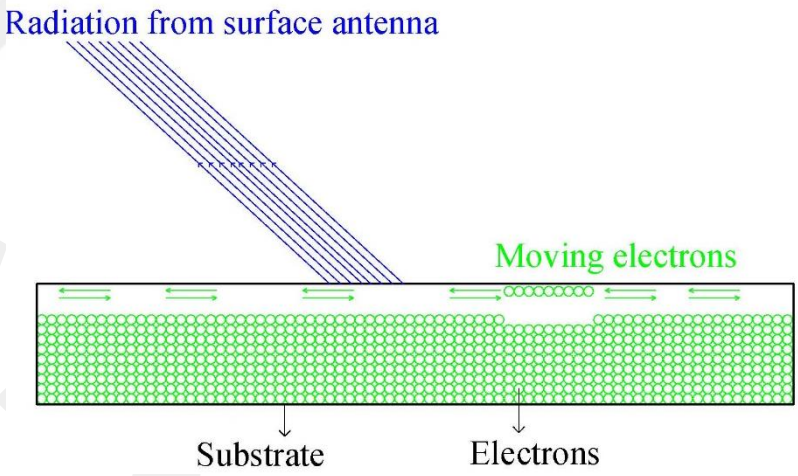

Figure 12 Detection of radiation from OA surface

Figure 12 shows in detection of radiation from OA surface which detected in optical radiation which means small wavelength between 200-400 nm. Optical radiation detects through photodetector.

3.2 Structure of an Optical Antenna

Researches are studied in several about structure of OAs which are used different semiconductors. There are gold (Au), silicon (Si), copper (Cu), lead sulfide (PbS), molybdenum disulphide (MoS_2) and silicon dioxide (SiO_2). The researches, in the first experiment of OA was occurred in [49] the dipole antenna semiconductor layers which were SiO_2 and Au. Parameters of DA were length of 260 nm, wide of 45nm, thick of 25 nm and gap of 15nm which shows in top view OA Figure 13. Dimension of layers were 20-150 nm thick of SiO_2, 600 nm thick of Si which shows in side view OA Figure 14.

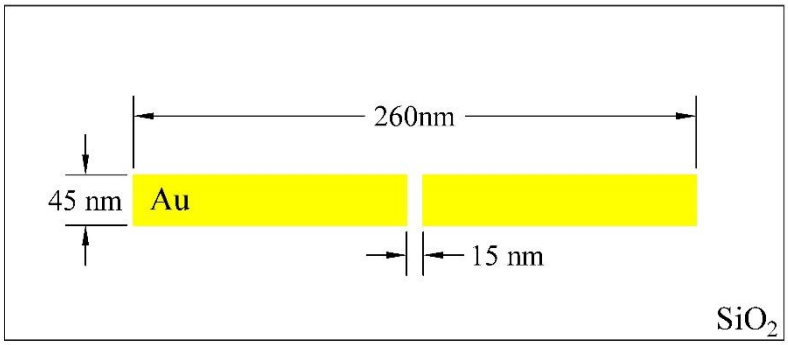

Figure 13 Top view in optical antenna

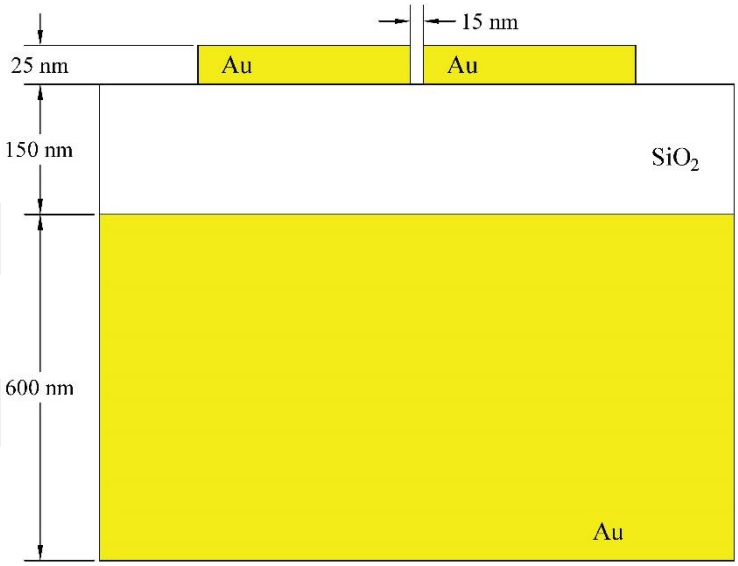

Figure 14 Side view in optical antenna

Result of first experiment was observed on optimum matching from thickness 80 nm. The parameter was dielectric spacer which means thickness. The result was observation good reflectance.

Second experiment was designed in [50] the array of cubes shape. The structures had been 4 layer which bottom layer BK7 silica glass, second layer gold (Au), third layer germanium-antimony-tellurium ($Ge_2Sb_2Te_5$), top layer gold. Design of layers were made that thickness of BK7 silica glass was 200 μm, thickness of gold was 100nm and thickness of germanium-antimony-tellurium was 25 nm. Design of these layer shows in side view Figure 15.

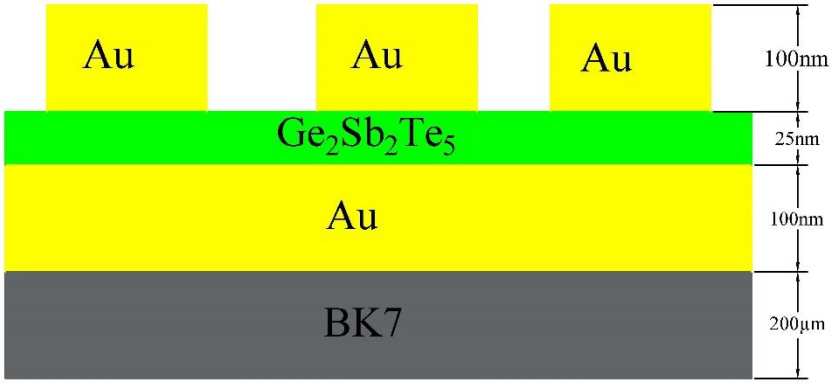

Figure 15 Side view of layers

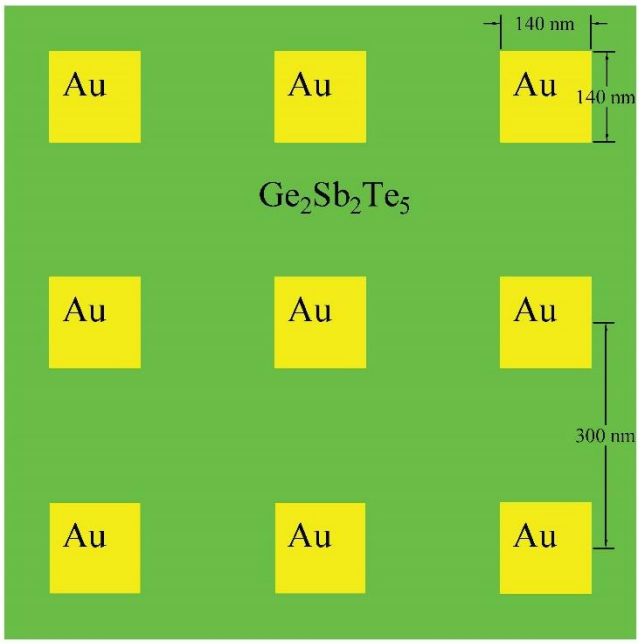

Figure 16 Top view of optical antenna

Figure 16 shows in top view of OA which dimension 140 nm in shape of square, center distances from each other is 300 nm. Result of second experiment was observed perfect absorber in the visible and near-infrared regions from OA. According to the experiment, application areas found in energy harvesting, biology and optical storage.

Third experiment was designed in [51] the patch antenna. The structure of patch antenna was included in 3 layers which were gold and substrate. The dimensions were 270x270 nm shape of square and were thickness 50 nm. The structure of patch antenna shows in the 3D view in Figure 17. Figure 18 shows in the side view of patch antenna.

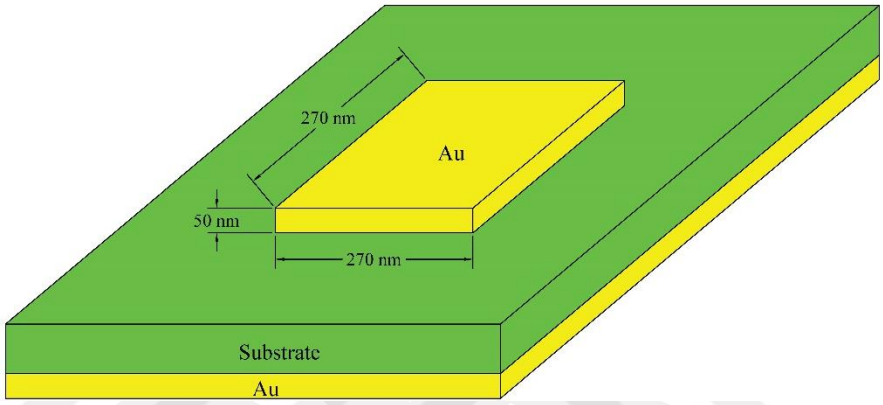

Figure 17 3D view of patch antenna

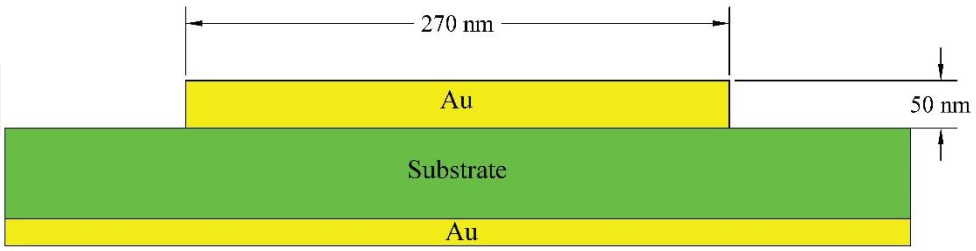

Figure 18 Side view of patch antenna

Result of third experiment had realized analysis, design and operation of optical patch antenna which was using the Cavity Model.

Fourth experiment was searched in [52] the dipole antenna trilayer semiconductors which were lead sulfide (PbS), molybdenum disulphide (MoS_2). This experiment was researched in the absorptance wavelength range from dipole antenna. Reason of

trilayer dipole antenna, the location of the semiconductors was raised amount to absorption. Structure of layers were the bottom layer silicon (Si), the middle layer silicon dioxide (SiO_2), top layer lead sulfide (PbS) includes shape of quantum dot and molybdenum disulphide (MoS_2) includes shape of dipole. The structure of layers shows in Figure 19.

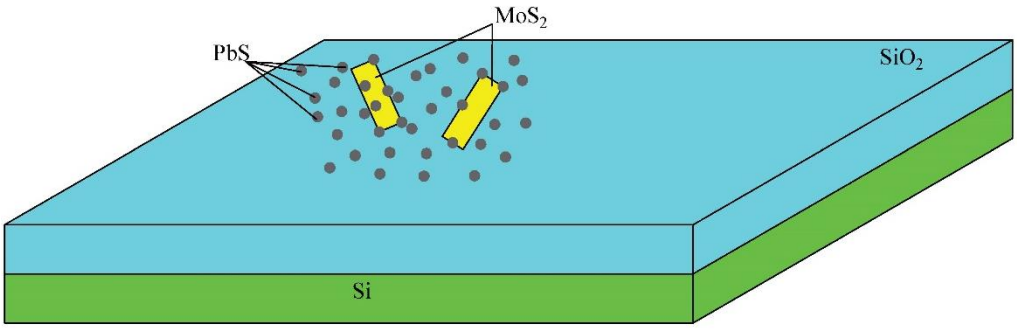

Figure 19 The structure of layers

While layers were generating for the antenna, used to production techniques which chemical vapor deposition and coating. Firstly, layer of $SiO_2$was placed over Si and PbS was shape of flakes over SiO_2 and MoS_2 was shape of dipole over SiO_2. Result of this experiment was observed absorptances in the wavelength range of 450-850 nm.

Result of structure of layers from optical antennas had used to production techniques. Their production techniques talk next in the section.

3.3 Production Techniques of Optical Antennas

Design of OAs has been careful dimensions, shapes and layers. Production techniques of OAs were Electron Beam Lithography (EBL), Ion Beam (IB). Using these techniques have designed the structures of OAs [53].

Electron Beam Lithography is an important technique for designing small electronic circuits. The technique is scanned a beam of electron across a surface coated with a resist film. The resist film is required on electrons saving energy in the substrate [54]. The electrons energy is reacted in absorption in the substrate [55]. The features

of EBL are very high resolution in atomic levels, an adaptable technology that is working a different materials and infinite number of electrons. Implementation of EBL is applied on over 2 layers which are Si and Au in Figure 20. A laser beam is sent to dissolve the Au on the Si. The Au is provided in dipole shape in Figure 21.

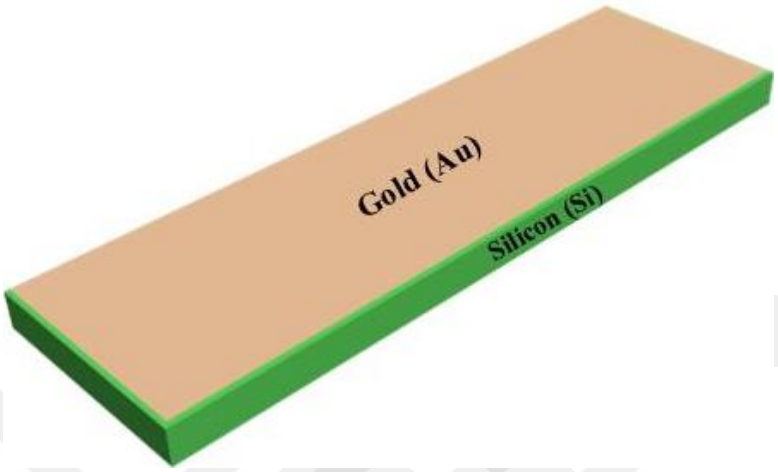

Figure 20 Layers of Si and Au

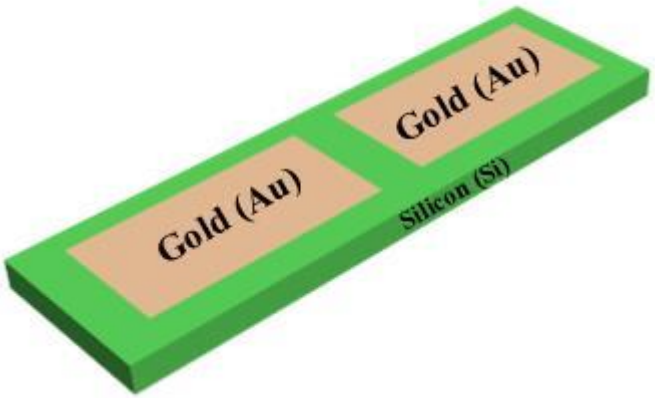

Figure 21 Optical dipole antenna

Ion Beam techniques is interacted between energetic ions and matter in the semiconductor. The energetic ions are sent in semiconductor that separated in electrons of atom and occurred electron cavity which placed different electrons in semiconductor [56]. Implementation of IB is applied on first a layer which is Si in Figure 22. Energetic ions are sent to deposition on the Si for electron empties. The

electron empties are putted in rectangular shape the electron of Au in Si substrate in Figure 23.

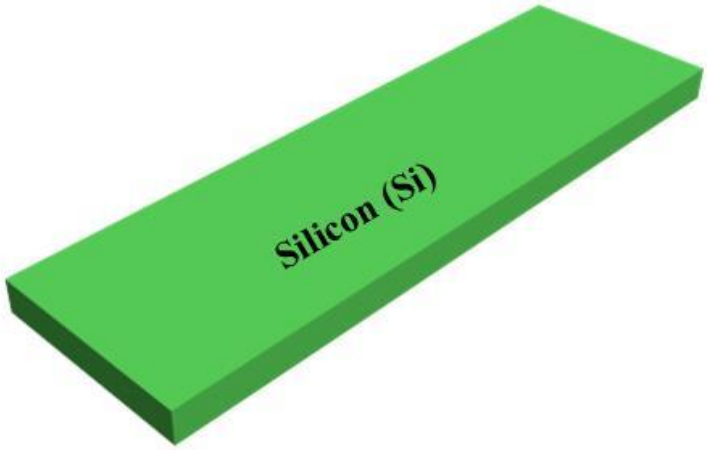

Figure 22 Layer of Si

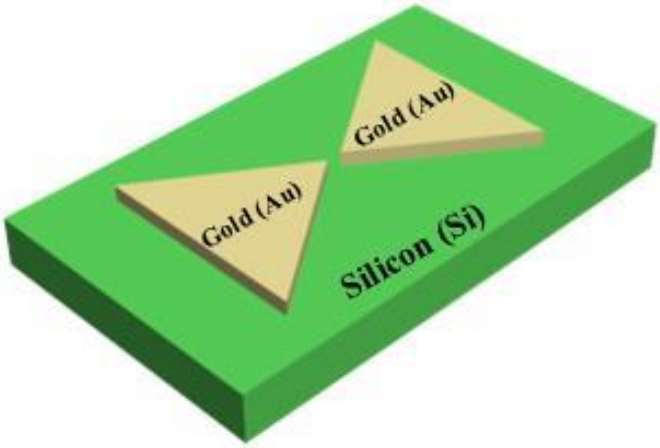

Figure 23 Optical bow-tie antenna

Process of design of OAs are chosen substrate for EBL. Substrates consists of 2 layers which are Si and Au. After layer of Si is placed on the film, layer of Au is placed on same way on the layer of Si. Laser beams are sent on the Au layer and the optical dipole antenna occur on the Au layer. Design of OAs are process for IB. First substrate is the Si. The substrate is given the rectangular shape though energetic ions. Electron

empties are sent electrons of Au in the semiconductor. End of the process occur optical bow-tie antenna on the substrate.

3.4 Application of Optical Antenna

In recent years, developing in technology had been applications of OAs which are wide area in the literature. There are five different applications such as photodetector [20-57], light emission [58-59], sensing [60], heat transfer [61-62] and spectroscopy [63-64].

For photodetector, was used in [20] the germanium material. The experiment was researched in conversion energy from photons to electrons. Photodetector was described in dipole antenna. Research was realized on wide bandwidth in this type photodetector. Another the research photodetector includes on [57] experiment and simulations. This research was used on same germanium material previous in the experiment. Photodetector was designed in the shape of nanowire which was dimension from 245 to 280 nm for numerical simulation. This experiment was observed on the role of interface between photonics and electronic. End of the experiment was observed on well agreement with numerical simulation which was high-speed operation (>100GHz) and low power consumption.

For light emission, was used in [58] the gold material. The research was included on experiment and simulation. The research was designed on bow-tie and dipole antenna which were shape of nanorods. These designs had small gap which was less than 30 nm. Used laser wavelength was 830 nm. End of the experiment, researches were studying visible, mid, and far-field, realized on that laser antenna had been many applications of area which are optical storage data, near- field optical microscopes and heat-assisted magnetic recording. Another light emission research was thin-film solar cell [59]. The experiment was used the silicon material and designed of silicon-on-insulator cell. Parameters of silicon-on-insulator were having 16 layers, designing of dipole-waveguide model and silicon wavelength 1250 nm. Thick of layer was separated on dimension 1.25 μm. The experiment was observed on interface between

incident photons and was inside of silicon electron from shape of silicon-on-insulator and occurred photocurrent enhancement. In the results of the experiment were resulted in that smaller metal particles were provided maximum overall rising from near-infrared for solar cell application and larger metal particles have more beneficial for light emission from thin-film solar cell.

In the use as sensing of optical sensor which was based on [60] metal nanoparticles and single nanoparticles. The experiment for sensing was applied on localized surface plasmon resonance method. This method is used on sensitivity size, shape, environment and detects molecular binding event and in molecular structures. End of the experiment was resulted on observation molecular events for application of chemical.

For heat transfer, was established in [61] the experimental setup which contained of coupling mirrors, parabolic mirrors, visible light beamsplitter and infrared beamsplitter, white light source, heater, polarizer, detector. Researchers had seen in the observation Transverse Electric (TE) and Transverse Magnetic (TM) modes for high temperature in the experiment. According to this result of the experimental setup was described on TE and TM modes which were $TE_0/TM_{\pm1}$ and $TE_{\pm1}$ that was observed lower frequencies from high temperature. In another experiment for heat transfer was used in [62] near-field scanning optical microcopy method which applied on using visible, infrared, terahertz, gigahertz ranges. The experiment sample was used to technique of electromagnetic local density of states, detected heat transfer from sample. Result of the experiment observed on sample $T=170^0C$, had given good results which were incident radiation wavelength 10.9 μm with 1 μm bandwidth.

For spectroscopy, had studied in [63] applying in the near-field technique. Researchers were established in the experimental setup which was designed optical dipole antenna. Cause of design of optical dipole antenna is calculations, observations easily. The experiment was observed on the exciting field from same frequency. Result of the experiment had understood spectroscopy technique on the optical dipole antenna. Spectroscopy method suggested in [64] from optical antenna by Fischer &

Pohl. The method used on gold film dipole antenna which observed on Scanning Near-Field Optical Microscopy (SNOM) from the antenna. Result of the experiment realized on new opportunities from the SNOM and described in the SNOM from gold film dipole antenna.

The mentioned above applications of optical antenna include on wide application areas in the literature. Each work resulted that would be applications of optical antenna in the future technology and would researched on this applications.

CHAPTER 4

DESIGN OF OPTICAL ANTENNA

4.1 Physical Optics

Physical Optics (PO) was proposed in [65] by McDonald in 1912. The method has used on calculation for the scattered field from a conducting and high-frequency technique. The PO has observed on surface current from perfectly conducting body. This surface was determined in the Geometrical Optics (GO) from the obstacles. GO means that electromagnetic waves are traveled in ray at high-frequencies. By means of GO method, the surface current is calculated. GO and PO are related each other's. The supposed PO surface current can be written;

$$\vec{J}_{PO} = \vec{n} x \vec{H}_{Total} \text{ , in the lit region} \tag{4.1}$$

and

$$\vec{J}_{PO} = 0 \text{ , in the shadow region} \tag{4.2}$$

where $\vec{n}$ is unit vector which is outward from the illuminated parts of scatter. $\vec{H}_{Total}$ is the total magnetic field intensity that described on the scatters field from obstacles. Lit and shadow regions according to Eq. (4.1) and Eq. (4.2) shows in Figure 24.

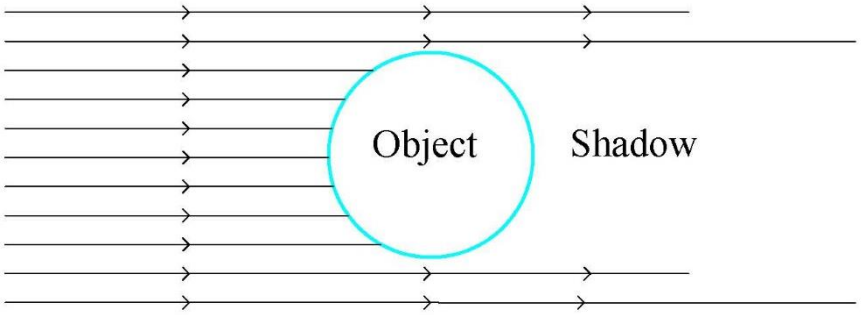

Figure 24 Physical optics lit and shadow regions

PO receives the reflected as GO fields, the total magnetic field on the surface of obstacle is double of incident field. Therefore, PO current is determined by

$$\vec{J}_{PO} = 2(\vec{n}x\vec{H}_i) \tag{4.3}$$

In the far field total scattering PO is described by

$$\vec{E}_s^{PO} = -j\omega\vec{A} \tag{4.4}$$

where ω is an angular frequency and $\vec{A}$ is magnetic vector potential. For $\vec{A}$ is written by integral of physical optics scattering. This integral is written as

$$\vec{A} = \frac{\mu_0}{4\pi}\iint_{S'}\vec{J}_{PO}\frac{e^{-jkR}}{R}ds' \tag{4.5}$$

where μ_0 is free space permeability and $\vec{J}_{PO}$ is current induced by the incident field and $\frac{e^{-jkR}}{R}$ is wave propagation from in the outward direction [66]. The radiated field is observed with integral of PO that are various design of OAs. These OAs are Optical Dipole Antenna (ODA), Optical Triangle Antenna (OTA), Optical Circular Antenna (OCA) and Optical Quarter Circular Antenna (OQCA).

4.2 Optical Dipole Antenna

Optical Dipole Antenna (ODA) observes in the X-Y coordinates. Parameters of ODA are width 70 nm from X coordinate, length 140 nm from Y coordinate axis. Wavelength of incident photon is 820 nm. Before incident electric field ($\vec{E}_i$) determines in the coordinate axis, surface current ($\vec{J}_{es}$) calculates through the converting $\vec{E}_i$ to $\vec{H}_i$ on the z=0 axis. End of this process is calculated in the magnetic vector potential ($\vec{A}$). ODA shows in Figure 25 in the y-z coordinates.

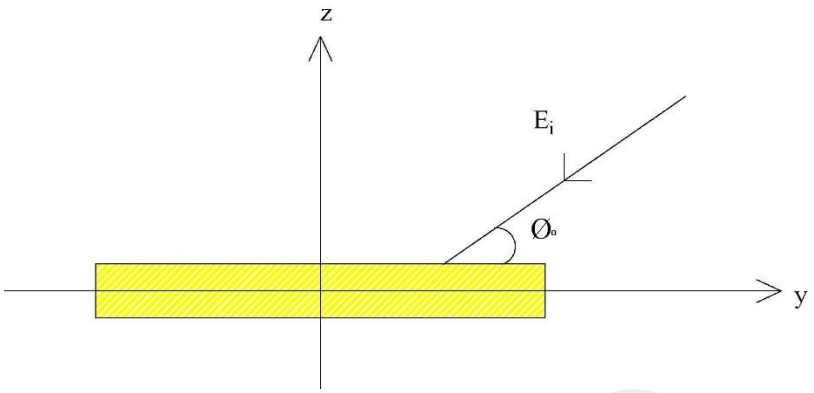

Figure 25 Optical dipole antenna in the y-z coordinates

Incident electric field ($\vec{E}_i$) can be written equation as Eq. (4.6)

$$\vec{E}_i = e^{jkz}\vec{e}_x E_0 \tag{4.6}$$

Eq. (4.6) includes in that $\vec{e}_x$ is incident wave polarization, direction of incident wave (e^{jkz}), the complex amplitude factor (E_0). Incident electric field ($\vec{E}_i$) is calculated in through these units. It requires converting $\vec{E}_i$ to $\vec{H}_i$ for surface current ($\vec{J}_{es}$). Converted $\vec{E}_i$ to $\vec{H}_i$ can be described as Eq. (4.7)

$$\vec{H}_i = -\frac{1}{j\omega\mu_0}\nabla x\vec{E}_i \tag{4.7}$$

Using Eq. (4.7) is placed in the Eq. (4.7) that can be written as

$$\vec{H}_i = -\frac{E_0}{j\omega\mu_0}\begin{vmatrix} \vec{e}_x & \vec{e}_y & \vec{e}_z \\ 0 & 0 & \frac{d}{dz} \\ e^{jkz} & 0 & 0 \end{vmatrix} \tag{4.8}$$

End of Eq. (4.8) is

$$\vec{H}_i = -\frac{E_0}{j\omega\mu_0}\left(-\vec{e}_y\frac{d}{dz}e^{jkz}\right) = \vec{e}_y\frac{E_0 k}{\omega\mu_0}e^{jkz} \tag{4.9}$$

Description of Z_0 can be written as Eq. (4.10)

$$Z_0 = \frac{\omega\mu_0}{k} \tag{4.10}$$

where c is speed of light equal to $c = \frac{1}{\sqrt{\varepsilon_0\,\mu_0}}$. k is wave number equal to $k = \frac{\omega}{c}$. Eq. (4.10) is placed in Eq. (4.10) that find $\vec{H}_i$;

$$\vec{H}_i = \vec{e}_y \frac{E_0 k}{Z_0} e^{jkz} \tag{4.11}$$

Surface current ($\vec{J}_{es}$) can be defined as Eq. (4.12)

$$\vec{J}_{es} = 2\vec{n}x\vec{H}_i \Big|_{z=0} \tag{4.12}$$

$\vec{n}$ is the unit normal vector equal to $\vec{e}_y$. Eq. (4.12) is putted in Eq. (4.11) that find $\vec{J}_{es}$ in the z=0;

$$\vec{J}_{es} = 2\vec{e}_z x\left(\vec{e}_y \frac{E_0 k}{Z_0} e^{jkz}\right)\Big|_{z=0} \tag{4.13}$$

As a result of $\vec{J}_{es}$ is found in Eq. (4.14)

$$\vec{J}_{es} = -\frac{2E_0}{Z_0}\vec{e}_x \tag{4.14}$$

Magnetic vector potential Eq. (4.5) is placed in Eq. (4.14)

$$\vec{A} = -\frac{\mu_0 E_0}{2\pi Z_o}\vec{e}_x \int_{x'=-a}^{x'=a}\int_{y'=-b}^{y'=b} \frac{e^{-jkR}}{R} dy'\,dx' \tag{4.15}$$

Dimension of $x^{\prime}$ are between a to $-a$ and dimension of $y^{\prime}$ is between b to $-b$. R is the ray path which Eq. (4.16) can be written as

$$R = \sqrt{(x-x')^2 + (y-y')^2 + (z-z')^2} \tag{4.16}$$

where apply far-field approximation that x', y', z' equals to zero.

$$R = \sqrt{(x')^2 + (y')^2 + (z')^2 + (x)^2 + (y)^2 + (z)^2 - 2xx' - 2yy'} \tag{4.17}$$

Definition of x and y can be written as

$$x = r\cos\phi\sin\theta \tag{4.18}$$

$$y = r\sin\phi\sin\theta \tag{4.19}$$

Calculation of Eq. (4.17) continues

$$R = \sqrt{r^2 - 2(xx' + yy')} = r\sqrt{1 - 2\left(\frac{xx' + yy'}{r}\right)} \tag{4.20}$$

where x and y are placed in Eq. (4.20) that R is found in approximation Eq. (4.21)

$$R \cong r - x'\cos\phi\sin\theta - y'\sin\phi\sin\theta \tag{4.21}$$

Eq. (4.15) is placed in Eq. (4.21)

$$\vec{A} = -\frac{\mu_0 E_0}{\pi Z_o}\vec{e}_x \frac{e^{-jkr}}{r}\int_{x'=-a}^{x'=a}\int_{y'=-b}^{y'=b} e^{jkx'\cos\phi\sin\theta} e^{jky'\sin\phi\sin\theta} dy'\,dx' \tag{4.22}$$

Calculation of Eq. (4.22) continues that result of $\vec{A}$ is Eq. (4.23)

$$\vec{A} = -\frac{\mu_0 E_0}{\pi Z_o}\vec{e}_x \frac{e^{-jkr}}{r}\frac{\sin(ka\sin\theta\cos\phi)}{ka\sin\theta\cos\phi}\frac{\sin(ka\sin\theta\sin\phi)}{ka\sin\theta\sin\phi} \tag{4.23}$$

Radiation pattern of ODA observes in Chapter 5. Calculation of magnetic vector potential observes different solution in the ODA which is described in height (h), length (L) in the x-y coordinates that shows in Figure 25.

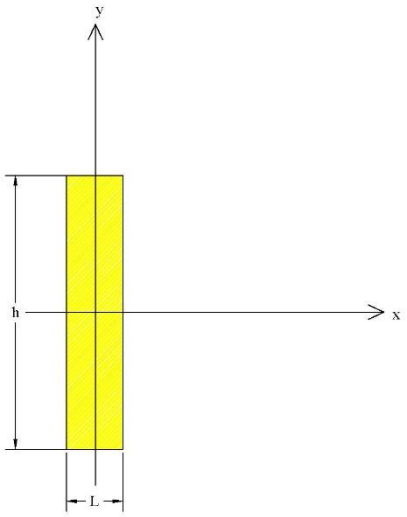

Figure 26 Optical dipole antenna in the x-y coordinates

The analysis of antenna in Figure 26 is different calculation method which height of antenna divides small pieces. These small pieces determine in delta that as

$$\delta = \frac{h}{N} \tag{4.24}$$

where h is height of ODA, N is segments of number of pieces. It determines in $y' = n\delta$ which describes in how pieces of delta (δ) from height of ODA. Equations of (4.2),

(4.8), (4.14) are used in the same solutions that are incident electric field ($\vec{E}_i$), incident magnetic field ($\vec{H}_i$), Surface current ($\vec{J}_{es}$). Magnetic vector potential of ODA can be written in the Eq. (4.25)

$$\vec{A} = \frac{\mu_0}{4\pi}\vec{e}_x \sum_{n=0}^{N-1} \int_{x'=-\frac{Ln}{2}}^{x'=\frac{Ln}{2}} \int_{y'=0}^{y'=\delta} \frac{e^{-jkR}}{R} dy'\,dx' \tag{4.25}$$

where x' is length of ODA that equals to $x' = \frac{Ln}{2}$. Magnetic vector potential describes in with serial formula. R is the ray path for the ODA which Eq. 4.26 can be written;

$$R = \sqrt{(x - x^{\iota})^2 + (y - y^{\iota})^2 + (z - z^{\iota})^2} \tag{4.26}$$

where x', y', z' equals to zero.

$$R = \sqrt{(x')^2 + (y')^2 + (z')^2 + (x)^2 + (y)^2 + (z)^2 - 2xx' - 2yy'} \tag{4.27}$$

where $y' = n\delta$ placed in Eq. (4.27)

$$R = \sqrt{r^2 - 2xx' - 2y\delta} \tag{4.28}$$

where are using Eq. (4.18) and Eq. (4.19) that can be written as

$$R = r\sqrt{1 - \frac{2(x'\cos\phi\sin\theta + \delta\sin\phi\sin\theta}{r}} \tag{4.29}$$

where R is found in approximation Eq. (4.30)

$$R \cong r - x'\cos\phi\sin\theta - \delta\sin\phi\sin\theta \tag{4.30}$$

As a result of R can be found in the Eq. (4.30). that put in Magnetic vector potential ($\vec{A}$) Eq. (4.25) that can be written as

$$\vec{A} = \frac{\mu_0}{4\pi}\vec{e}_x \sum_{n=0}^{N-1} \frac{e^{-jkr}}{r} e^{jk\delta\sin\phi\sin\theta} \int_{x'=-\frac{Ln}{2}}^{x'=\frac{Ln}{2}} e^{jkx'\cos\phi\sin\theta} dx' \tag{4.31}$$

The exponential function converts series formula that can be describes in the Eq. (4.32)

$$e^x = \sum_{n=0}^{\infty} \frac{x^n}{n!} \tag{4.32}$$

If x<<1, can be written;

$$e^x = 1 + x + \frac{x^2}{2} + \frac{x^3}{6} + \frac{x^4}{24} + \ldots \tag{4.33}$$

The Eq. (4.33) is placed in Eq. (4.30)

$$\vec{A} = \frac{\mu_0}{4\pi}\vec{e}_x \sum_{n=0}^{N-1} \frac{e^{-jkr}}{r} e^{jk\delta \sin\phi \sin\theta}\left(1 - \frac{jkLn\sin\theta\cos\phi}{2}\right) \tag{4.34}$$

Result of $\vec{A}$ can be resulted in the Eq. (4.34).

4.3 Optical Triangle Antenna

Optical Triangle Antenna (OTA) observes in the x-y coordinates. Parameters of ORA are width 70 nm from x coordinate, length 140 nm from y coordinate axis. Wavelength of incident photon is 820 nm. Before incident electric field ($\vec{E}_i$) determines in the coordinate axis, surface current ($\vec{J}_{es}$) calculates through the converting $\vec{E}_i$ to $\vec{H}_i$ on the z=0 axis. End of this process is calculated in the magnetic vector potential ($\vec{A}$). ORA shows in Figure 26 in the x-y coordinates.

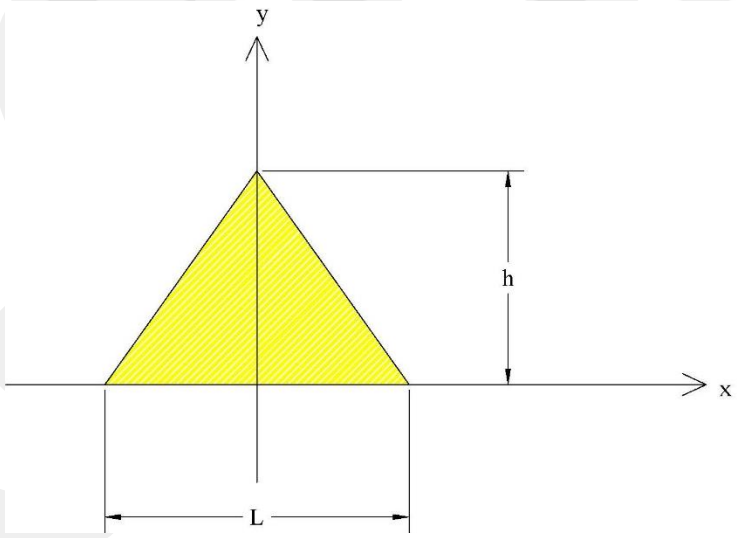

Figure 27 Optical triangle antenna in the X-Y coordinates

The analysis of antenna in Figure 27 is same calculation method which height of antenna divides small pieces. These small pieces determine in delta in the Eq. (4.24). Equations of (4.6), (4.8), (4.14) are used in the same solutions that are incident electric

field ($\vec{E}_i$), incident magnetic field ($\vec{H}_i$), Surface current ($\vec{J}_{es}$), piece of delta (δ). Angle of triangle is equal to

$$\alpha = \tan^{-1}\left(\frac{Lh}{2}\right) \tag{4.35}$$

Magnetic vector potential of OTA can be written in the Eq. (4.36)

$$\vec{A} = -\frac{\mu_0}{4\pi}\vec{e}_x \sum_{n=0}^{N-1} \int_{x'=-\frac{L(N-n)}{\tan\alpha}}^{x'=\frac{L(N-n)}{\tan\alpha}} \int_{y'=0}^{y'=n\delta} \frac{e^{-jkR}}{R} dy'dx' \tag{4.36}$$

R is the ray path for the OTA which Eq. (4.16) where $z' = 0$ in the Eq. (4.26) where $y' = n\delta$ placed in the Eq. (4.26). Definition of x and y can be written polar coordinates as

$$x = r\cos\phi\sin\theta \tag{4.37}$$

$$y = r\sin\phi\sin\theta \tag{4.38}$$

According to Eq. (4.37) and Eq. (4.38), R can be written as

$$R = \sqrt{r^2 - 2r\left(x'\cos\phi\sin\theta + n\delta\sin\phi\sin\theta\right)} \tag{4.39}$$

where R is found in approximation as

$$R \cong r - x'\cos\phi\sin\theta - y'\sin\phi\sin\theta \tag{4.40}$$

As a result of R shows in the Eq. (4.40) which is placed in the Eq. (4.36)

$$\vec{A} = -\frac{\mu_0}{4\pi}\vec{e}_x \sum_{n=0}^{N-1} e^{jkn\delta\sin\phi\sin\theta} \frac{e^{-jkr}}{r} \int_{x'=-\frac{L(N-n)}{\tan\alpha}}^{x'=\frac{L(N-n)}{\tan\alpha}} e^{jkx'\sin\theta\cos\phi} dx' \tag{4.41}$$

Eq. (4.41) solves in

$$\vec{A} = -\frac{\mu_0}{4\pi}\vec{e}_x \sum_{n=0}^{N-1} e^{jkn\delta\sin\phi\sin\theta} \frac{e^{-jkr}}{r}\left(1 - \frac{jkL(N-n)\sin\theta\sin\phi}{\tan\alpha}\right) \tag{4.42}$$

Result of $\vec{A}$ can be resulted in the Eq. (4.42)

4.4 Optical Circular Antenna

Optical Circular Antenna (OCA) observes in the X-Y coordinates. Parameters of OCA is radius 140 nm from X coordinate. Wavelength of incident photon is 820 nm. Before incident electric field ($\vec{E}_i$) determines in the coordinate axis, surface current ($\vec{J}_{es}$) calculates through the converting $\vec{E}_i$ to $\vec{H}_i$ on the z=0 axis. End of this process is calculated in the magnetic vector potential ($\vec{A}$). OCA shows in Figure 28 in the x-y coordinates.

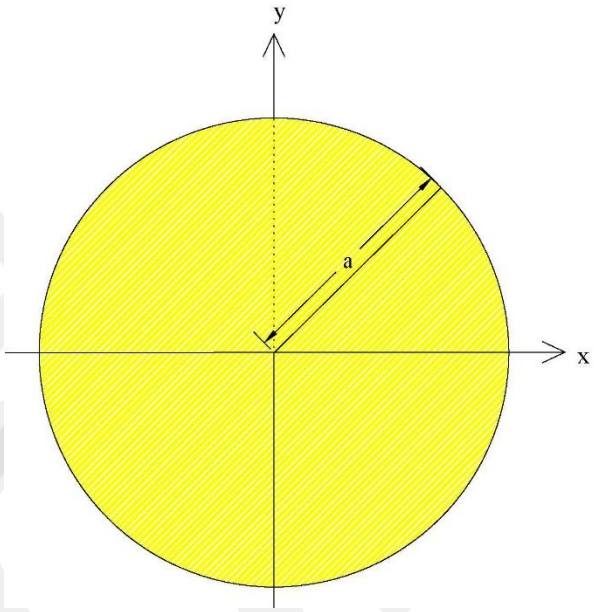

Figure 28 Optical circular antenna in the x-y coordinates

The magnetic vector potential ($\vec{A}$) describes on from OCA;

$$\vec{A} = \frac{\mu_0 I_0}{4\pi} \vec{e}_\phi \int_{\rho'=0}^{\rho'=a} \int_{\phi'=0}^{\phi'=2\pi} \frac{e^{-jkR}}{r} \rho' d\rho' d\phi' \tag{4.43}$$

R is the ray path for the OCA which equals to

$$R = \sqrt{(x-x')^2 + (y-y')^2 + (z-z')^2} \tag{4.44}$$

where x, y and ρ are described in

$$x = \rho \cos \emptyset \tag{4.45}$$

$$y = \rho \ \sin \emptyset \tag{4.46}$$

$$\rho = r \ \sin \theta \tag{4.47}$$

Eq. (4.45) and Eq. (4.46) is placed in the Eq. (4.44) where $z' = 0$

$$R = \sqrt{(\rho \cos\phi - \rho' \cos\phi')^2 + (\rho \sin\phi - \rho' \sin\phi')^2 + z^2} \tag{4.49}$$

where calculation of Eq. (4.49) continues

$$R = \sqrt{\rho^2 + z^2 + (\rho')^2 - 2\rho\rho' \cos(\phi - \phi')} \tag{4.50}$$

where neglectable $(\rho^{\prime})^2$ and Eq. (4.47) place in the Eq. (4.50)

$$R = \sqrt{r^2 - 2\rho' r \sin\theta \cos(\phi - \phi')} \tag{4.51}$$

where R is found in approximation as

$$R \cong r - \rho' \sin\theta \cos(\phi - \phi') \tag{4.52}$$

As a result of R shows in the Eq. (4.52) where is placed in the Eq. (4.43)

$$\vec{A} = \frac{\mu_0 I_0}{4\pi} \vec{e}_\phi \frac{e^{-jkr}}{r} \int_{\rho'=0}^{\rho'=a} \int_{\phi'=0}^{\phi'=2\pi} e^{jk\rho' \sin\theta \cos(\phi - \phi')} \rho' d\rho' \, d\phi' \tag{4.53}$$

where a is radius of OCA which equals to

$$a = n\delta \tag{4.54}$$

where δ describes in that radius of this OCA divides in small pieces which equals to

$$\delta = \frac{a}{N} \tag{4.55}$$

Included in the Eq. (4.53) convert in the Bessel Generate Function which described as

$$e^{\frac{1}{2}z\left(t - \frac{1}{t}\right)} = \sum_{n=-\infty}^{\infty} J_n(z) t^n \tag{4.56}$$

where z and t are equal to;

$$z = k\rho' \sin\theta \tag{4.57}$$

$$t = \cos(\phi - \phi') \tag{4.58}$$

Eq. (4.57) and Eq. (4.58) are putted in the Eq. (4.56) which can be written as

$$e^{jk\rho'\sin\theta\cos(\phi-\phi')} = \sum_{n=-\infty}^{\infty} J_0(k\rho'\sin\theta)(\cos(\phi-\phi'))^n \tag{4.59}$$

As a result of Bessel Generate Function can be written;

$$e^{jk\rho'\sin\theta\cos(\phi-\phi')} = \sum_{n=-\infty}^{\infty} J_0(k\rho'\sin\theta)2\pi \tag{4.60}$$

Eq. (4.60) is placed in the Eq. (4.55) as

$$\vec{A} = \frac{\mu_0 I_0}{4\pi}\vec{e}_\phi 2\pi \frac{e^{-jkR}}{r}\int_{\rho'=0}^{\rho'=n\delta} J_0(k\rho'\sin\theta)\rho' d\rho' \tag{4.61}$$

The definition of derivative described in

$$\lim_{\Delta\to 0}\int_a^{\Delta+a} f(x)dx = \lim_{\Delta\to 0}\frac{F(x+\Delta)+F(x)}{\Delta} = f(a) \tag{4.62}$$

According to the Eq. (4.62), resulted of the Eq. (4.61) can be written as

$$\vec{A} = \mu_0 I_0 \vec{e}_\phi \frac{e^{-jkr}}{r}\sum_{n=1}^{N-1} n\delta J_0(kn\delta\sin\theta) \tag{4.63}$$

End of the magnetic vector potential ($\vec{A}$) is in the Eq. (4.63).

4.5 Optical Quarter Circular Antenna

Optical Quarter Circular Antenna (OQCA) observes in the x-y coordinates. Parameters of OQCA is radius 140 nm from X coordinate. Wavelength of incident photon is 820 nm. Before incident electric field ($\vec{E}_i$) determines in the coordinate axis, surface current ($\vec{J}_{es}$) calculates through the converting $\vec{E}_i$ to $\vec{H}_i$ on the z=0 axis. End of this process is calculated in the magnetic vector potential ($\vec{A}$). OQCA shows in Figure 29 in the x-y coordinates.

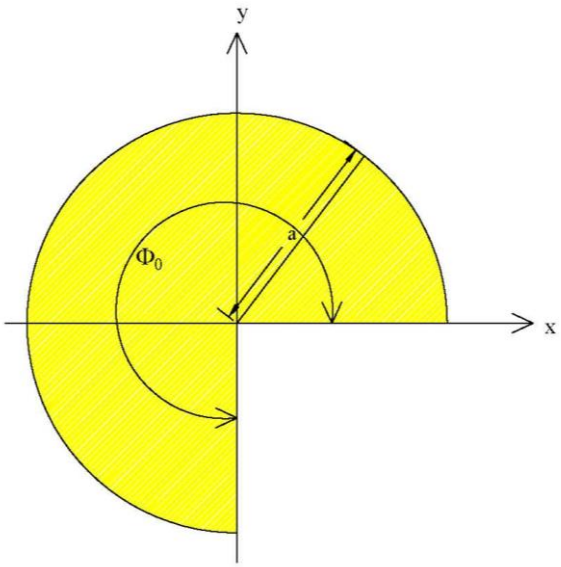

Figure 29 Optical quarter circular antenna in the x-y coordinates

Equations of (4.44), (4.45), (4.46), (4.47), (4.52), (4.54), (4.55) are used in the same solutions that are incident electric field ($\vec{E}_i$), piece of delta (δ). Resulted in their equations are described in magnetic vector potential ($\vec{A}$)

$$\vec{A} = \frac{\mu_0 I_0}{4\pi} \vec{e}_\phi \frac{e^{-jkr}}{r} \int_{\rho'=0}^{\rho'=a} \int_{\phi'=0}^{\phi'=\phi_0} e^{jk\rho' \sin\theta \cos(\phi-\phi')} \rho' d\rho' d\phi' \tag{4.64}$$

where a equals to $n\delta$ that can be written as

$$\vec{A} = \frac{\mu_0 I_0}{4\pi} \vec{e}_\phi \frac{e^{-jkr}}{r} \int_{\phi'=0}^{\phi'=\phi_0} \sum_{n=1}^{N-1} n\delta e^{jkn\delta \sin\theta \cos(\phi-\varphi')} d\phi' \tag{4.65}$$

The Eq. (4.33) use in the Eq. (4.65) which can be written as

$$\vec{A} = \frac{\mu_0 I_0}{4\pi} \vec{e}_\phi \frac{e^{-jkr}}{r} \int_{\phi'=0}^{\phi'=\phi_0} \sum_{n=1}^{N-1} n\delta \left(1 + jkn\delta \sin\theta \cos(\phi-\phi')\right) d\phi' \tag{4.66}$$

where calculates in the Eq. (4.66) for $\emptyset'$ as

$$\vec{A} = \frac{\mu_0 I_0}{4\pi} \vec{e}_\phi \frac{e^{-jkr}}{r} \sum_{n=1}^{N-1} n\delta \left(\phi_0 - jkn\delta \sin\theta \left(\sin(\phi-\phi_0) - \sin\phi_0\right)\right) \tag{4.67}$$

Bessel Generate Function form converts in the Eq. (4.67)

$$\vec{A} = \frac{\mu_0 I_0}{4\pi} \vec{e}_\phi \frac{e^{-jkr}}{r} n\delta J_0(kn\delta \sin\theta)\left(\phi_0 - jkn\delta \sin\theta \left(\sin(\phi-\phi_0) - \sin\phi_0\right)\right) \tag{4.68}$$

As a result of the magnetic vector potential ($\vec{A}$) is in the Eq. (4.68).

The radiation diagrams of different design of optical antennas will be examined in Chapter 5 in the direction of these Eq. (4.23), Eq. (4.34), Eq. (4.42), Eq. (4.63), Eq. (4.68). These different designs of optical antennas will be observed in the radiation diagrams that are advantages and disadvantages. These observation parameters are coverage range, radiation intensity.

CHAPTER 5

RADIATION PATTERN OF OPTICAL ANTENNAS

5.1 Radiation Pattern of Optical Dipole Antenna

This section is focused on two solution analysis radiation pattern of Optical Dipole Antenna (ODA). First, the solution analysis with using the Eq. (4.23) at radiation patterns in different angles of ϕ' , lengths (b), heights (a) are observed in the ODA. In addition, radiation patterns are observed in the various angles which were 5˚, 10˚, 30˚, 45˚, 60˚ and 90˚ on the angle axes.

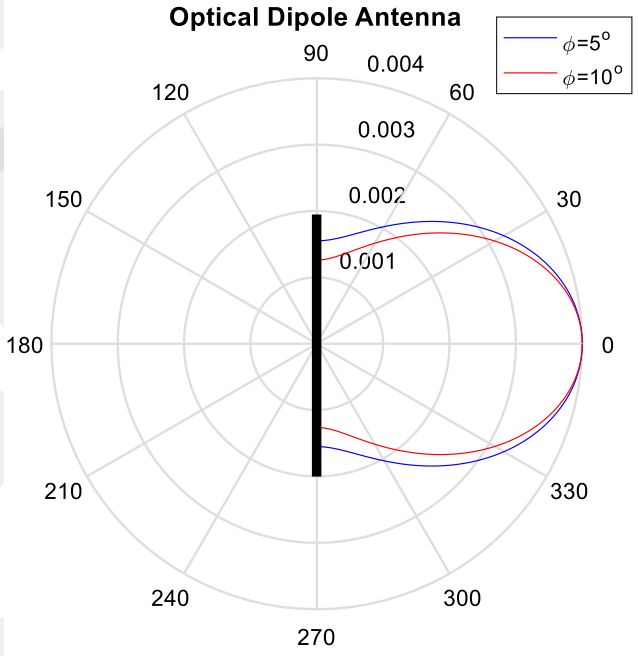

Figure 30 Radiation pattern of optical dipole antenna for $\phi' = 5^o$ and $\phi' = 10^o$

Figure 30 shows on the radiation pattern of optical dipole antenna for $\phi' = 5^o$ and $\phi' = 10^o$. The ODA is represented on wide coverage range by $\phi' = 5^o$. When ϕ' is raised, the coverage range is reduced.

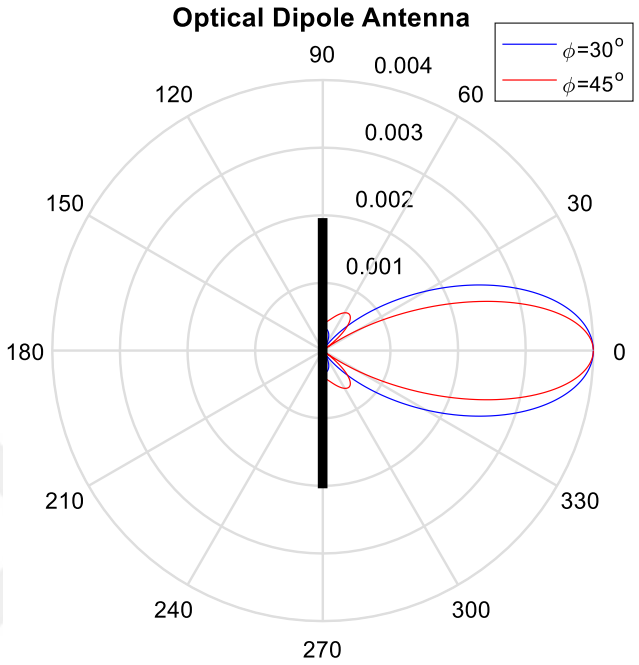

Figure 31 Radiation pattern of optical dipole antenna for $\phi' = 30^o$ and $\phi' = 45^o$

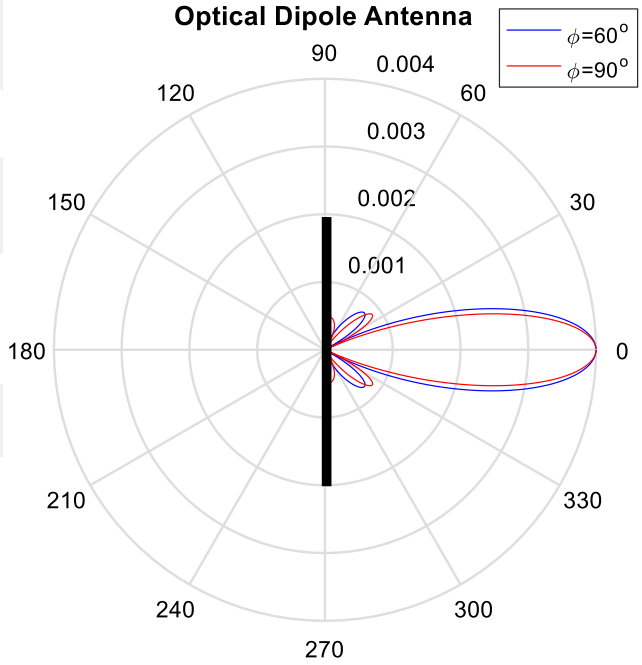

Figure 32 Radiation pattern of optical dipole antenna for $\phi' = 60^o$ and $\phi' = 90^o$

Figure 31 shows radiation pattern of optical dipole antenna for $\phi' = 30^o$ and $\phi' = 45^o$. The ODA is represented on wide coverage range by $\phi' = 30^o$. Especially, wide small beams are visible in the radiation pattern between the angles 60˚ to 330˚ from $\phi' = 45^o$. The maximum radiation is the angle 0˚ from $\phi' = 30^o$ and $\phi' = 45^o$. Figure 32 shows radiation pattern of optical dipole antenna for $\phi' = 60^o$ and $\phi' = 90^o$. The ODA is figured on wide coverage range by $\phi' = 60^o$. The small beams are visible in the radiation pattern between the angles 60˚ to 330˚ from $\phi' = 60^o$. As shown in Figure 32, small beams are composed of two pieces for $\phi' = 90^o$. The small beams are visible in the radiation pattern between the angles 30˚ to 60˚ and 300˚ to 330˚ from $\phi' = 90^o$.

The using the Eq. (4.23) at radiation patterns are observed on different lengths (a) and heights (b) from $\phi' = 30^o$ and $\phi' = 90^o$. These parameters are constant height, decreasing lengths and constant length, decreasing height. In the first observation is constant length and decreasing heights from $\phi' = 30^o$.

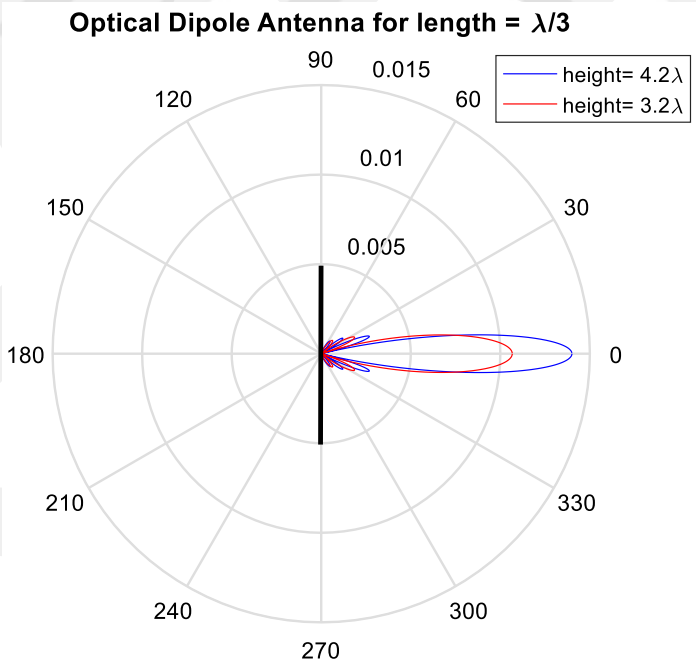

Figure 33 Radiation pattern of optical dipole antenna for length of $\lambda/3$, heights of 4.2λ and 3.2λ from $\phi' = 30^o$

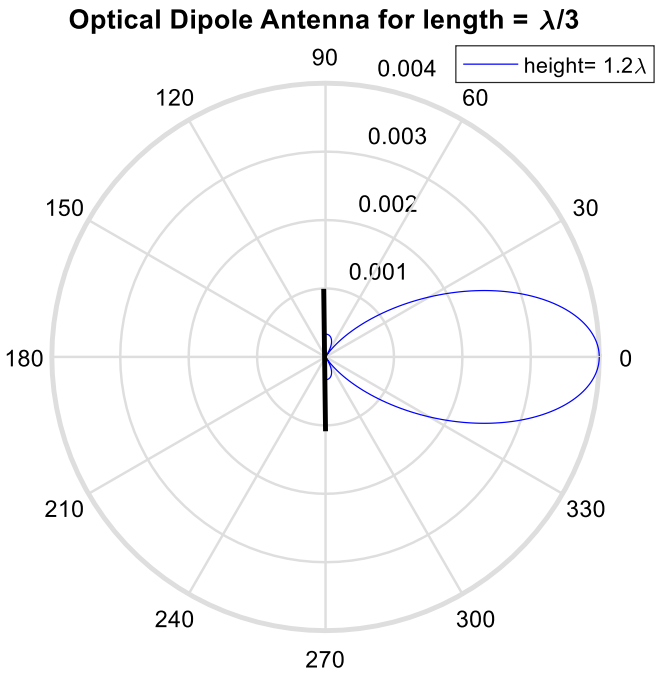

Figure 34 Radiation pattern of optical dipole antenna for length of $\lambda/3$ and height of 1.2λ from $\phi' = 30^o$

Figure 33 shows radiation pattern of ODA for length of $\lambda/3$, heights of 4.2λ and 3.2λ from $\phi' = 30^o$. As seen in Figure 33, the radiation field is decreasing at constant height and decreasing length. Small beams are primarily visible between the angles 30° to 330° and these beams approach the main beam at the 0° and maximum radiation is the angle 0° from heights of 4.2λ and 3.2λ. Figure 34 shows on radiation pattern of ODA for length of $\lambda/3$, height of 1.2λ from $\phi' = 30^o$. As seen Figure 34, the radiation field is decreasing as Figure 33. Main beam was the angle 0° from height of 1.2λ. Side beams are small in the height of 1.2λ. In the second observation is constant height and decreasing lengths from $\phi' = 30^o$. Figure 35 shows on radiation pattern of ODA for length of λ and height of 3.2λ from $\phi' = 30^o$. Figure 36 shows on radiation pattern of ODA for height of 3.2λ, lengths of $\lambda/4$ and $\lambda/8$ from $\phi' = 30^o$. As seen Figure 35 and Figure 36, the radiation field is decreasing at constant length and decreasing height. Small beams are primarily visible between the angles

60˚ to 300˚ from lengths of $\lambda/4$ and $\lambda/8$.Then, these beams approach the main beam at the 0˚ and maximum radiation is the angle 0˚ from lengths of λ , $\lambda/4$ and $\lambda/8$.

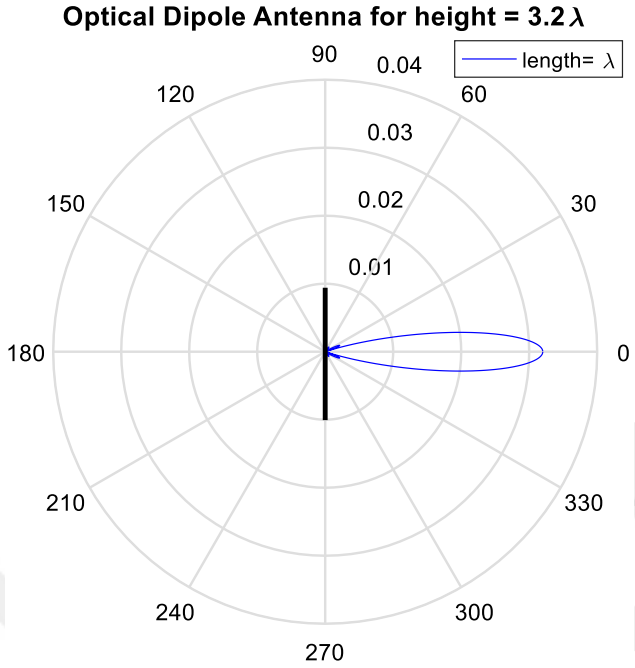

Figure 35 Radiation pattern of optical dipole antenna for height of 3.2λ and length of λ from $\phi' = 30^o$

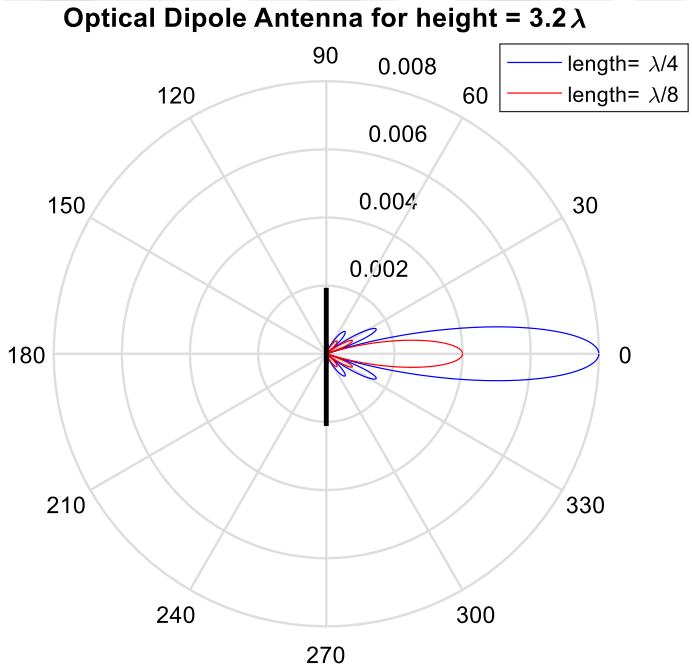

Figure 36 Radiation pattern of optical dipole antenna for height of 3.2λ , lengths of $\lambda/4$ and $\lambda/8$ from $\phi' = 30^o$

In the third observation was constant length and decreasing heights from $\phi' = 90^o$. Figure 37 shows on radiation pattern of ODA for length of $\lambda/3$, heights of 4.2λ and 3.2λ from $\phi' = 90^o$.

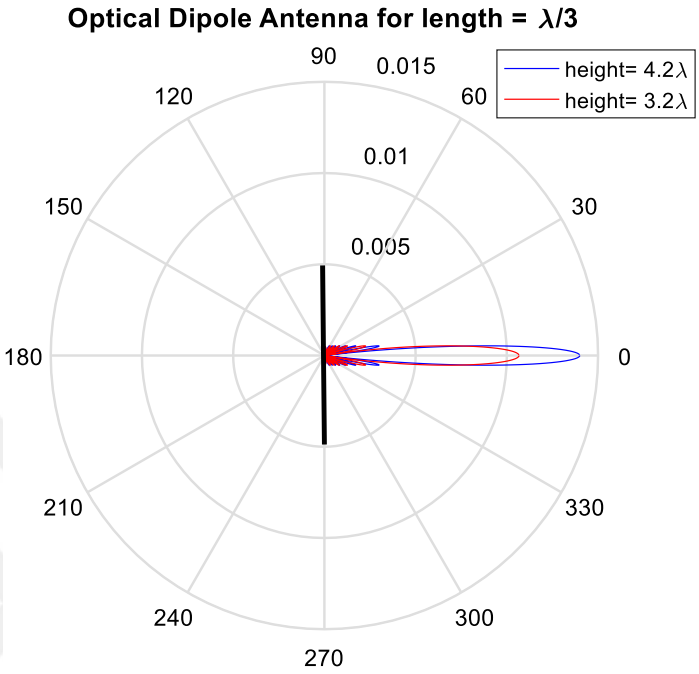

Figure 37 Radiation pattern of optical dipole antenna for length of $\lambda/3$, heights of 4.2λ and 3.2λ from $\phi' = 90^o$

As seen Figure 37, the radiation field is decreased at constant height and decreasing length. Small beams are primarily visible between the angles 30˚ to 330˚ from height of 4.2λ and 3.2λ. Then, these beams approach the main beam at the 0˚ and maximum radiation is the angle 0˚ from heights of 4.2λ and 3.2λ. Figure 38 shows on radiation pattern of ODA for length of $\lambda/3$, height of 1.2λ from Small beams are primarily visible between the angles 30˚ to 330˚ from height of 1.2λ. Then, these beams approach the main beam at the 0˚ and maximum radiation is the angle 0˚ from height of 1.2λ.

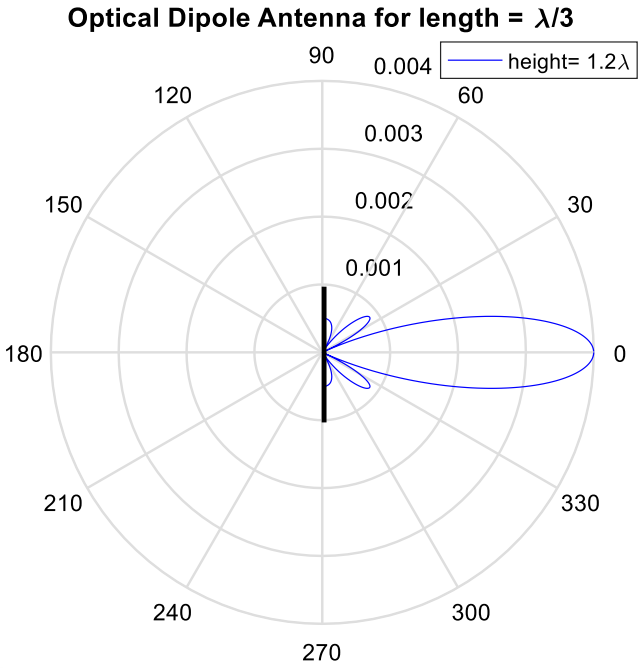

Figure 38 Radiation pattern of optical dipole antenna for length of $\lambda/3$, height of 1.2λ from $\phi' = 90^o$

In the fourth observation is constant height and decreased lengths from $\phi' = 90^o$. Figure 39 shows on radiation pattern of ODA for height of 3.2λ, and length of λ from $\phi' = 90^o$. Small beams are primarily visible between the angles 60° to 300° from length of λ. Then, these beams approach the main beam at the 0° and maximum radiation is the angle 0° from height of λ. Figure 40 shows on radiation pattern of ODA for height 3.2λ, lengths of $\lambda/4$ and $\lambda/8$ from $\phi' = 90^o$. Small beams are primarily visible between the angles 60° to 300° from length of $\lambda/8$. Then, these beams approach the main beam at the 0° and maximum radiation is the angle 0° from lengths of $\lambda/4$ and $\lambda/8$. As a result, radiation intensity was decreased in these observations, when heights and lengths were taken small dimension. Also, radiation intensity was increased in these observations, when heights and lengths was taken great dimension.

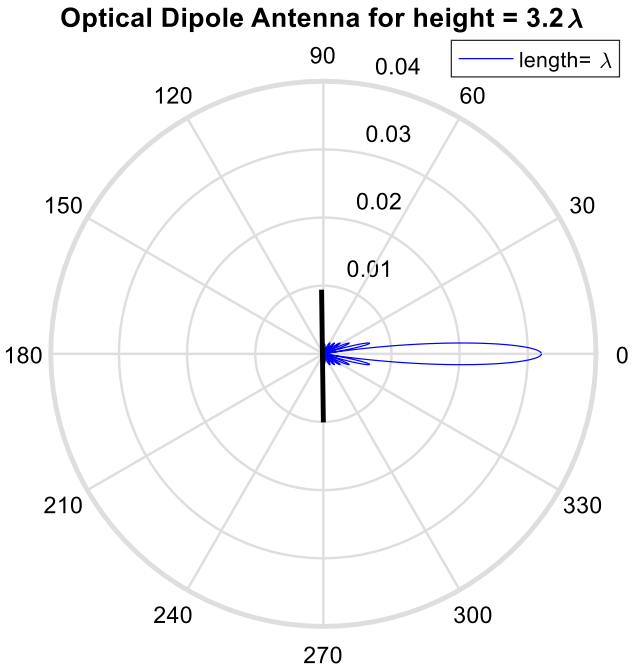

Figure 39 Radiation pattern of optical dipole antenna for height of 3.2λ and length of λ from $\phi' = 90^o$

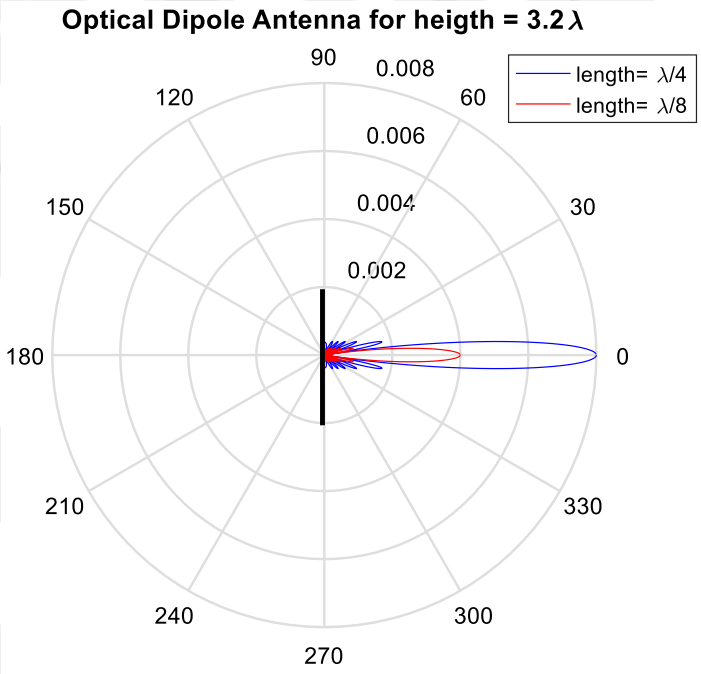

Figure 40 Radiation pattern of optical dipole antenna for height of 3.2λ and lengths of $\lambda/4$ and $\lambda/8$ from $\phi' = 90^o$

Second the solution analysis, the using the Eq. (4.34) at radiation patterns different in angles of ϕ', constant segments of number (N), lengths (L), heights (h)were observed in the ODA. The first observation was in different angles of ϕ' segments of number which were $N = 25$ and $N = 100$. Figure 41 shows on $\phi' = 5^o$, $\phi' = 10^o$ and $\phi' = 30^o$ for N=25.

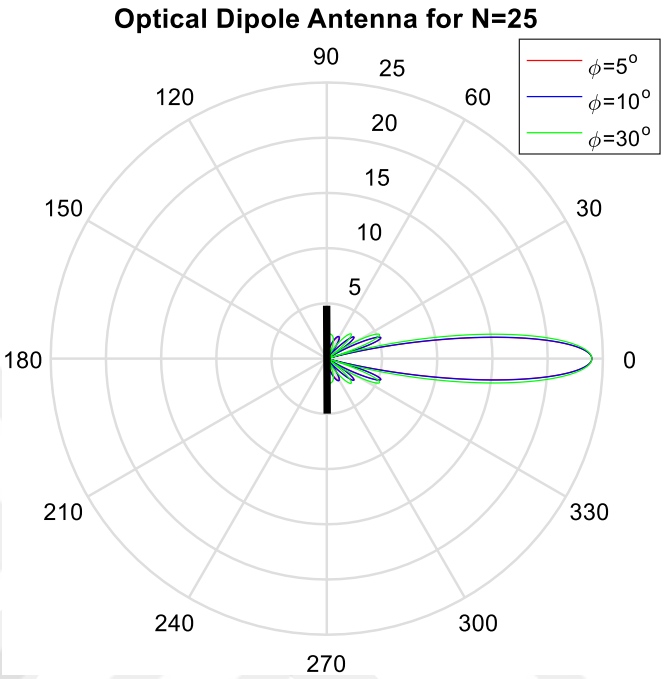

Figure 41 Radiation pattern of optical dipole antenna $N = 25$ for $\phi' = 5^o$, $\phi' = 10^o$ and $\phi' = 30^o$

As shown in Figure 41, radiation patterns are same graphs from $N = 25$ for $\phi' = 5^o$, $\phi' = 10^o$ and $\phi' = 30^o$. Small beams were primarily visible between the angles 60˚ to 300˚ from $N = 25$ and maximum radiation is the angle 0˚. Figure 42 shows on $\phi' = 45^o$, $\phi' = 60^o$ and $\phi' = 90^o$ for $N = 25$. As shown in Figure 42, small beams were primarily visible between the angles 60˚ to 300˚ for $\phi' = 45^o$ and other small beams were primarily visible between the angles 60˚ to 300˚ for $\phi' = 60^o$. Radiation patterns for $N = 25$ had been wide area for $\phi' = 90^o$.

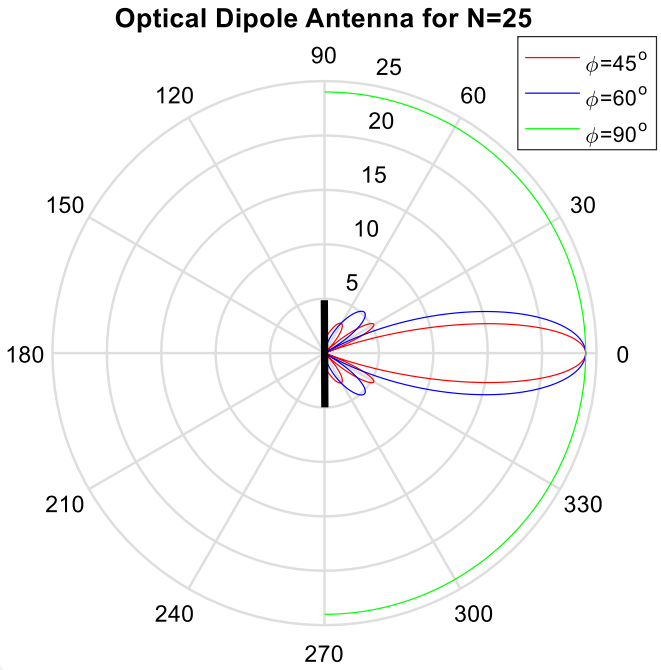

Figure 42 Radiation pattern of optical dipole antenna $N = 25$ for $\phi' = 45^{o}$, $\phi' = 60^{o}$ and $\phi' = 90^{o}$

Figure 43 shows on $\phi' = 5^{o}$, $\phi' = 10^{o}$ and $\phi' = 30^{o}$ for N=100.

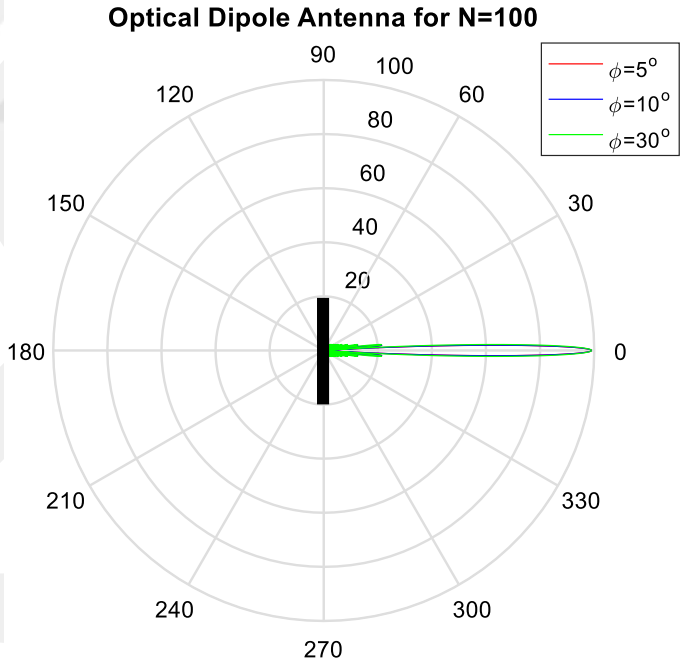

Figure 43 Radiation pattern of optical dipole antenna $N = 100$ for $\phi' = 5^{o}$, $\phi' = 10^{o}$ and $\phi' = 30^{o}$

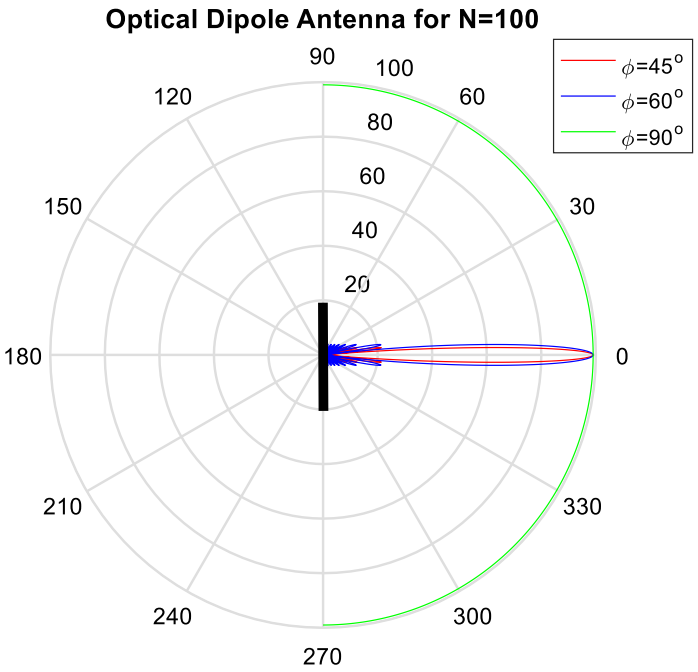

Figure 44 Radiation pattern of optical dipole antenna $N = 100$ for $\phi' = 45^{0}$, $\phi' = 60^{0}$ and $\phi' = 90^{0}$

As shown in Figure 44, radiation patterns are same graphs as Figure 43 from $N = 100$ for $\phi' = 5^{o}$, $\phi' = 10^{o}$ and $\phi' = 30^{o}$. Figure 44 shows on $\phi' = 45^{o}$, $\phi' = 60^{o}$ and $\phi' = 90^{o}$ for N=100. As shown in Figure 44, radiation patters are same graphs as $N = 100$ for $\phi' = 45^{0}$, $\phi' = 60^{0}$. Therefore, radiation patterns for $\phi' = 90^{0}$ have wide area. The reason for $N = 100$, when the value of N increases, the accuracy of the radiation pattern is observed in this ODA.

In the second observation is included constant height, become less the value of lengths, angle of $\phi' = 30^{o}$ and segment of number $N = 25$ for the second solution analysis. Figure 45 shows on height of 3.2λ and length of λ from $\phi' = 30^{o}$ and $N = 25$. As shown in Figure 45, small beams are primarily visible between the angles 60˚ to 300˚ for $\phi' = 30^{o}$. Maximum radiation is the angle 0˚. Figure 46 shows on height of 3.2λ and lengths of $\lambda/4$ and $\lambda/8$ from $\phi' = 30^{o}$ and $N = 25$. As shown in Figure 46, small beams are primarily visible between the angles 30˚ to 330˚ for $\lambda/8$. Therefore, beams for $\lambda/4$ have smaller than $\lambda/4$. Maximum radiation is the angle 0˚.

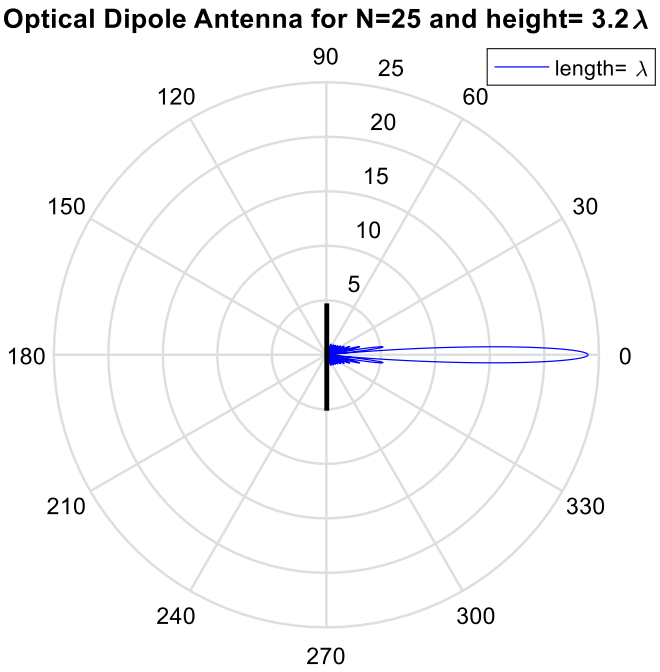

Figure 45 Radiation pattern of optical dipole height of 3.2λ and length of λ from $\phi' = 30^o$ and $N = 25$

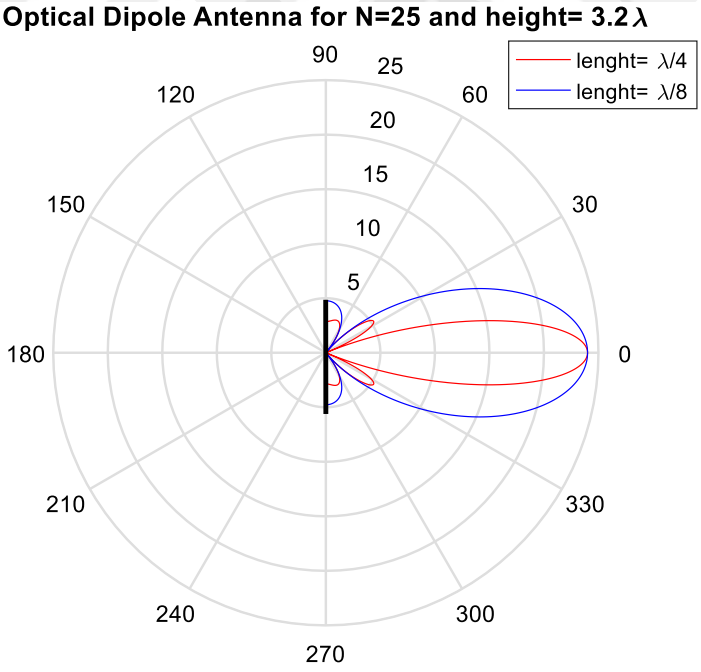

Figure 46 Radiation pattern of optical dipole height of 3.2λ and lengths of $\lambda/4$ and $\lambda/8$ from $\phi' = 30^o$ and $N = 25$

In the fourth observation is included in constant height and decreasing lengths for $\phi' = 30^o$ and $N = 100$. Figure 47 shows on height of 3.2λ and lengths of $\lambda/4$ and $\lambda/8$ from $\phi' = 30^o$ and $N = 100$.

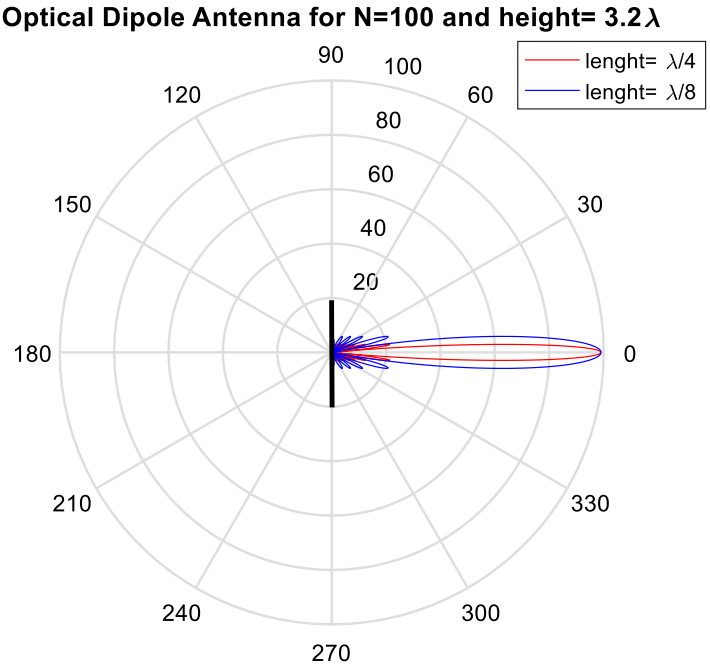

Figure 47 Radiation pattern of optical dipole height of 3.2λ and lengths of $\lambda/4$ and $\lambda/8$ from $\phi' = 30^o$ and $N = 100$

As shown in Figure 47, small beams are primarily visible between the angles 30˚ to 300˚ for $\lambda/8$. Therefore, beams for $\lambda/4$ have smaller than $\lambda/4$. Maximum radiation is the angle 0˚. Figure 46 and Figure 47 are similar radiation patterns for height of 3.2λ and lengths of $\lambda/4$ and $\lambda/8$. Another observation is included in constant length and decreasing heights for $\phi' = 30^o$ and $N = 25$. Figure 48 shows on length of 3.2λ and height of $\lambda/4$ from $\phi' = 30^o$ and $N = 25$. Figure 49 shows on length of 3.2λ and height of $\lambda/8$ from $\phi' = 30^o$ and $N = 25$. As shown in Figure 48 and Figure 49, radiation patterns are same graph each other. Because observation of radiation patterns are not affected constant length and decreasing heights. If number of segments are $N = 25$, radiation patterns was same as Figure 48 and Figure 49.

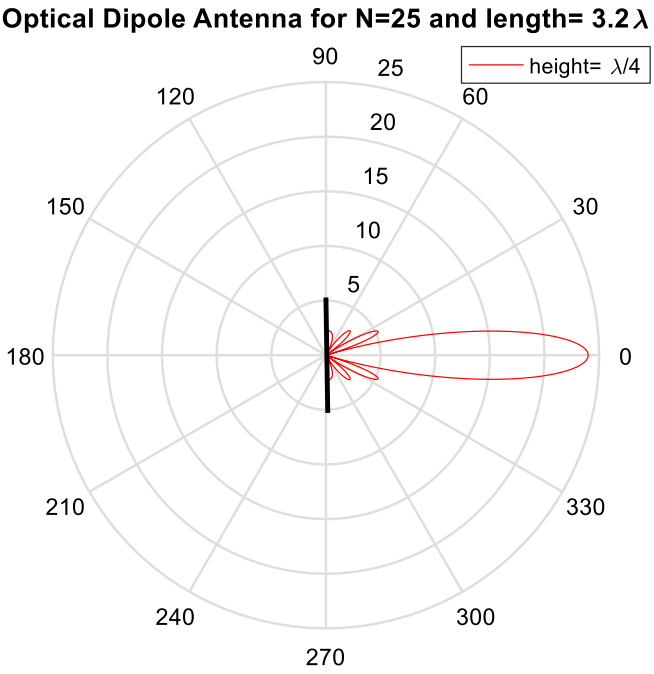

Figure 48 Radiation pattern of optical dipole length of 3.2λ and height of $\lambda/4$ from $\phi' = 30^o$ and $N = 25$

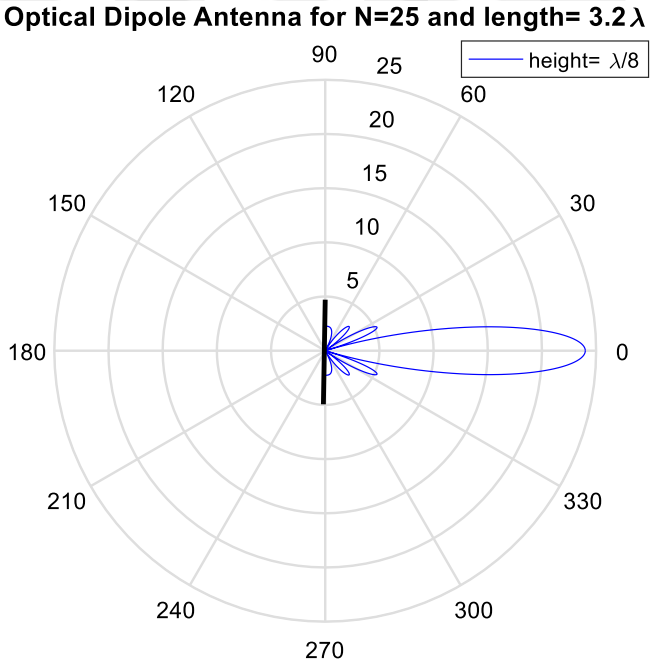

Figure 49 Radiation pattern of optical dipole length of 3.2λ and height of $\lambda/8$ from $\phi' = 30^o$ and $N = 25$

As a result of these observations, when the length and height values decrease with respect to the first solution analysis, the radiation field is decreased. On the other hand, when the height and length values of the optic antenna increase, the radiation field increases. At the same time, the maximum radiation at all observations is zero degrees. According to the second solution, as the height is taken constant, as the length value decreases, increasing in the radiant field is observed. But when the length is taken constant and the decreasing height, all the radiation patterns are the same. When the segment values increase, the accuracy of these antennas increase. In the last observation, the radiation diagram is the same even though the number of segments increases as in the Figure 48 and 49.

5.2 Radiation Pattern of Optical Triangle Antenna

In this section observes on radiation pattern from Optical Triangle Antenna (OTA). The using the Eq. (4.42) at radiation patterns different in angles of ϕ' constant segment of number (N), different lengths (L) and height (h) are determined in from ORA.

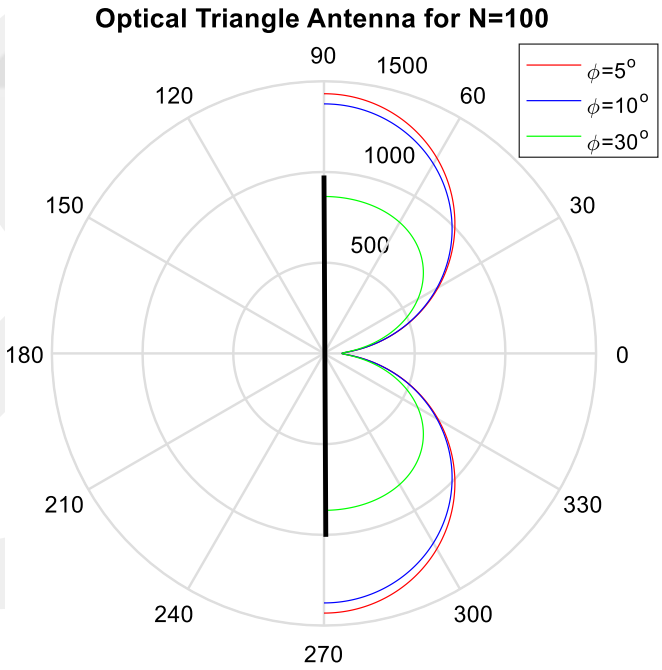

Figure 50 Radiation pattern of optical triangle antenna $N = 100$

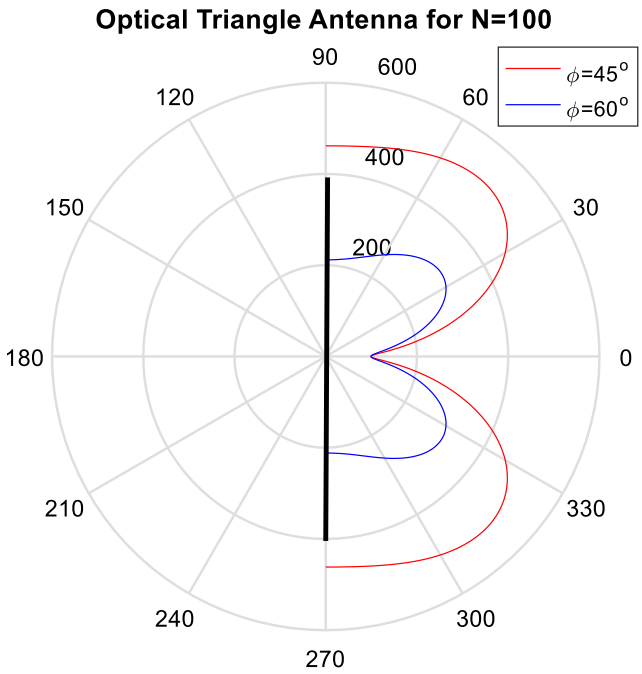

Figure 51 Radiation pattern of optical triangle antenna $N = 100$

In the first analysis is for different angles of ϕ' and constant segment of number (N). Figure 50 shows on $\phi' = 5^o$, $\phi' = 10^o$ and $\phi' = 30^o$ for $N = 100$. As shown in Figure 50, the observation radiation patterns have been different radiation area from $N = 100$ for $\phi' = 5^o$, $\phi' = 10^o$ and $\phi' = 30^o$. The radiation patterns of OTA have widest at $\phi' = 5^o$, lowest at $\phi' = 30^o$. Figure 51 shows on $\phi' = 45^o$, $\phi' = 60^o$ for $N = 100$. As shown in Figure 36, the observation radiation patterns have are different radiation area from $N = 100$ for $\phi' = 45^o$ and $\phi' = 60^o$. The radiation patterns of ORA are widest at $\phi' = 45^o$, lowest at $\phi' = 60^o$.Figure 52 shows on N=100 for $\phi' = 90^o$.

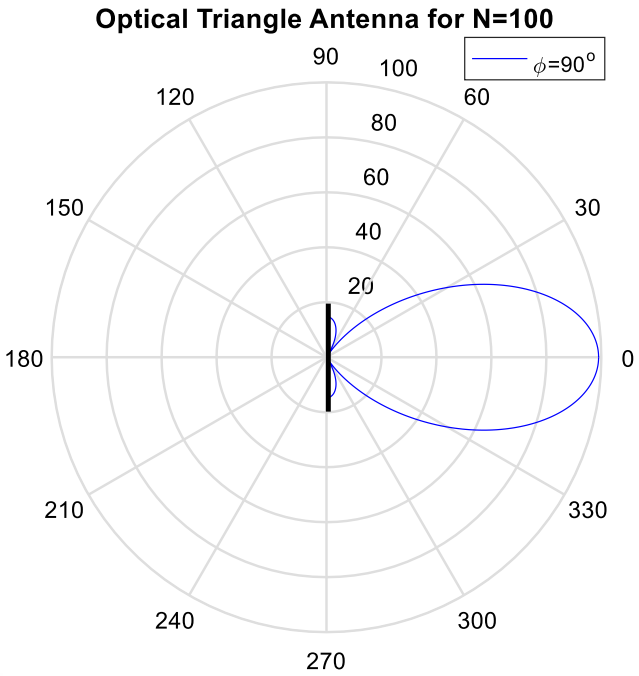

Figure 52 Radiation pattern of optical triangle antenna $N = 100$

As shown in Figure 52, the observation radiation patterns are different radiation area from $N = 100$ for $\phi' = 90^{o}$. Maximum radiation is the angle 0° but radiation intensity is between 0 to 100 from $\phi' = 90^{o}$.

In the second analysis is included in constant length and decreasing heights from $N = 100$. Figure 53 shows on length of $\lambda/3$, heights of 4.2λ and 3.2λ for $\phi' = 60^{o}$ and $N = 100$. As show in Figure 53, the observation radiation patterns have been wide coverage area and wide small beams. These small beams were primarily visible between the angles 90° to 270° for $\phi' = 60^{o}$ and height of 3.2λ. Another height of 4.2λ have narrow beams. Maximum radiation is the angle 0° both of heights. Figure 54 shows on length of $\lambda/3$, heights of 1.2λ for $\phi' = 60^{o}$ and $N = 100$. As shown in Figure 54, the observation radiation patterns have been wide coverage and high radiation intensity. Minimum radiation is the angle 0°.

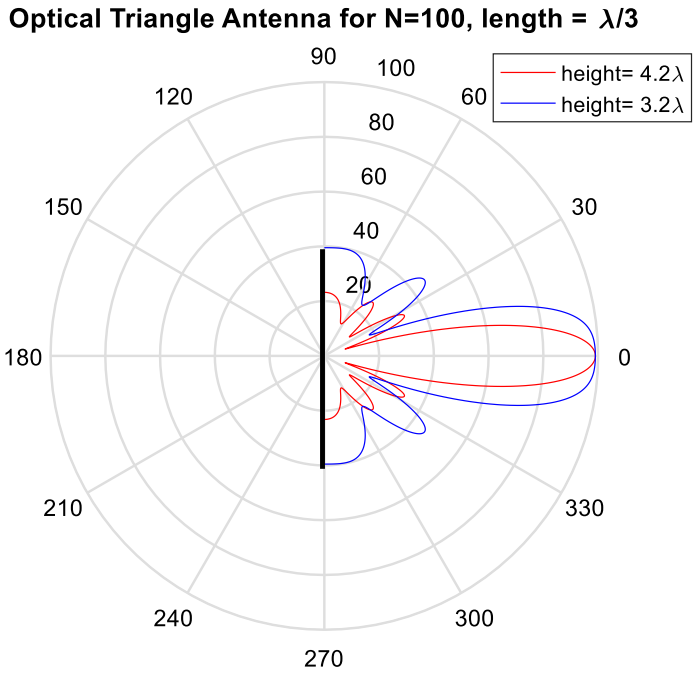

Figure 53 Radiation pattern of optical triangle antenna length of $\lambda/3$, heights of 4.2λ and 3.2λ for $\phi' = 60^o$

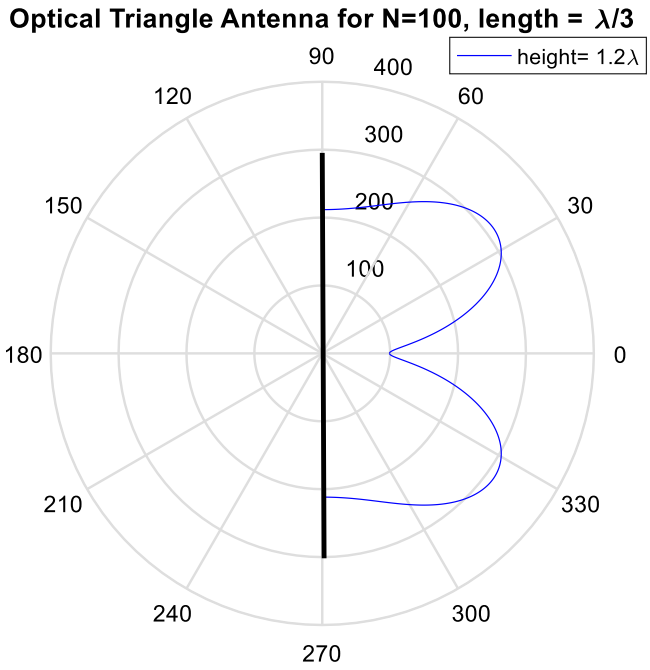

Figure 54 Radiation pattern of optical triangle antenna length of $\lambda/3$, height of 1.2λ for $\phi' = 60^o$

In the third analysis is included in constant height and decreasing lengths from $N=100$. Figure 55 shows on height of 3.2λ, lengths of $\lambda/4$ and $\lambda/8$ for $\phi^{'}=60^{o}$ and $N=100$. Figure 56 shows on height of 3.2λ, length of λ for $\phi^{'}=60^{o}$ and $N=100$. As seen Figure 55, the observation radiation patterns have been wide coverage area and wide small beams. These small beams are primarily visible between the angles 90˚ to 270˚ for $\phi^{'}=60^{o}$ and length of $\lambda/4$. Another height of $\lambda/8$ have narrow beams. Maximum radiation is the angle 0˚ both of lengths. As seen Figure 56, the observation radiation patterns are wide coverage area and have high radiation intensity.

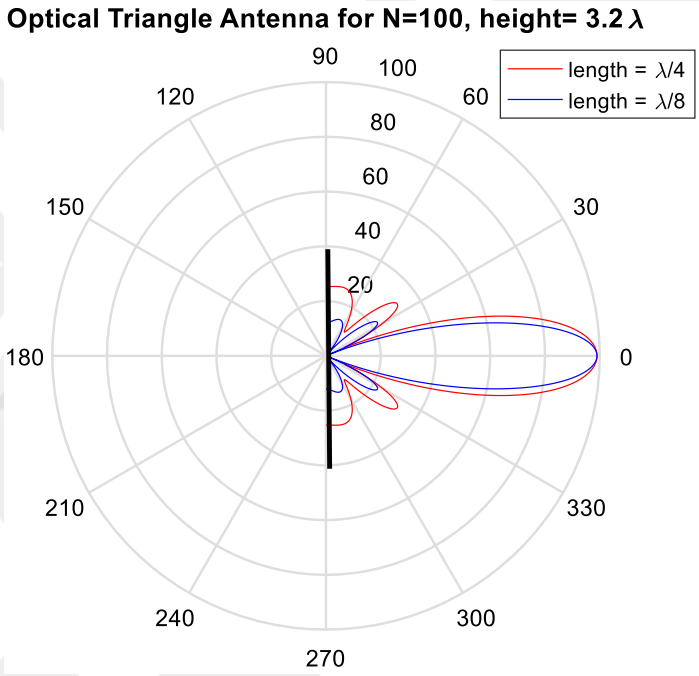

Figure 55 Radiation pattern of optical triangle antenna height of 3.2λ, lengths of $\lambda/4$ and $\lambda/8$ for $\phi^{'}=60^{o}$

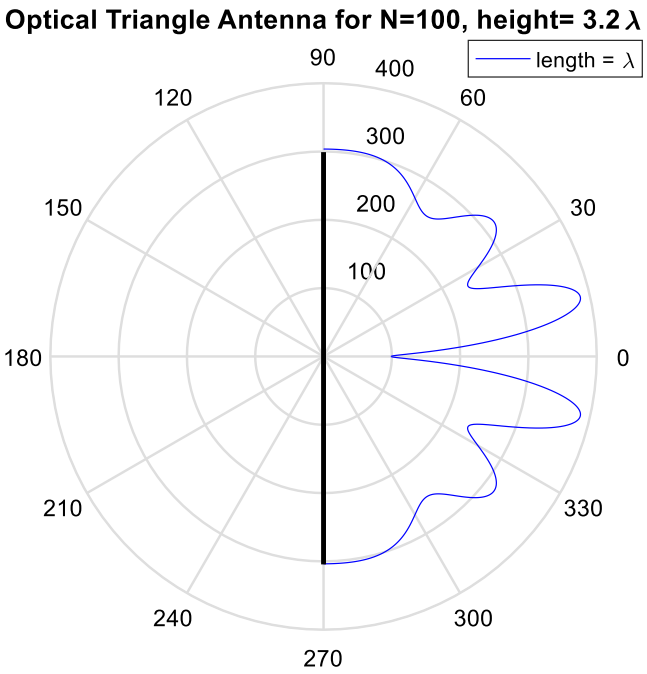

Figure 56 Radiation pattern of optical triangle antenna height of 3.2λ , length of λ for $\phi' = 60^0$

As a result of these observations, the length is fixed, while the height is reduced, the radiation field is higher. When the height is taken very low, the radiation field has a wide and a scattered area which is seen. The height is fixed, while the radiation field is the same when the length is reduced.

5.3 Radiation Pattern of Optical Circular Antenna

In this section observes on radiation pattern from Optical Circular Antenna (OCA). The using the Eq. (4. 63) at radiation patterns constant segments of number (N) and different radius (a) are determined in from OCA. Figure 57 shows on radius of 1.2λ for N=100. As seen Figure 57, the radiation field was contained in small beam which were primarily visible between the angles 60˚ to 300˚. Maximum radiation is the angle 0˚.

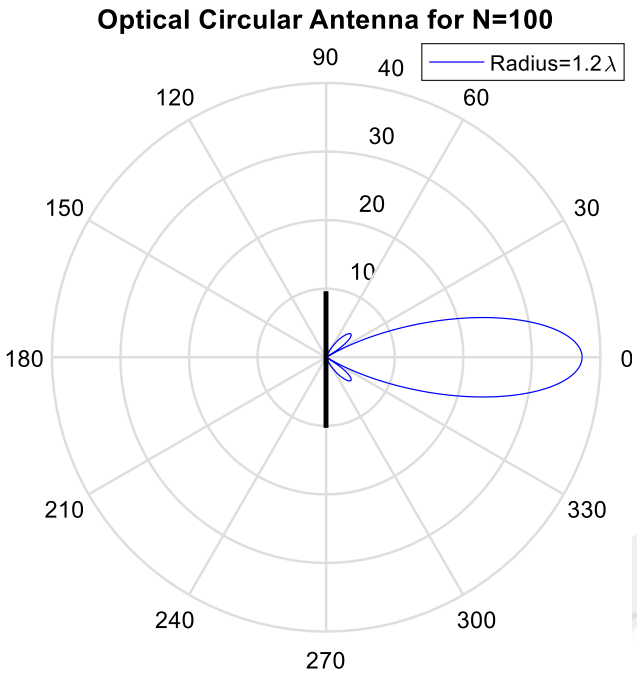

Figure 57 Radiation pattern of optical circular antenna radius of 1.2λ for N=100

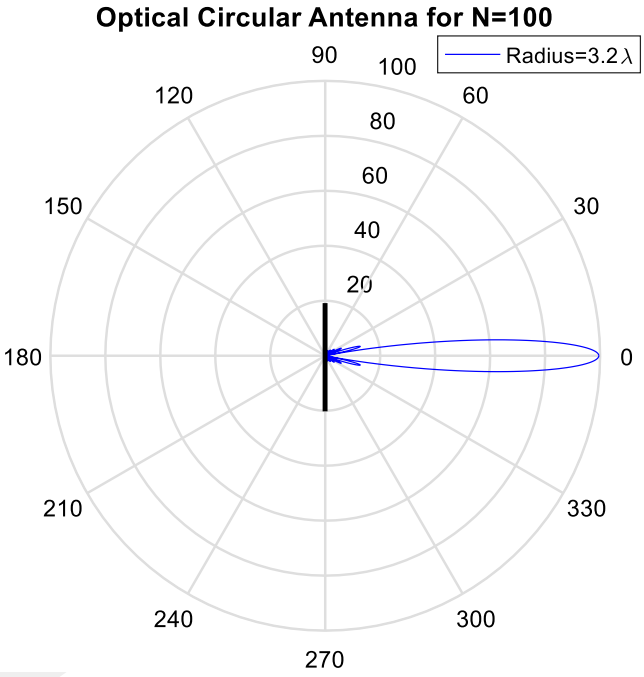

Figure 58 Radiation pattern of optical circular antenna radius of 3.2λ for N=100

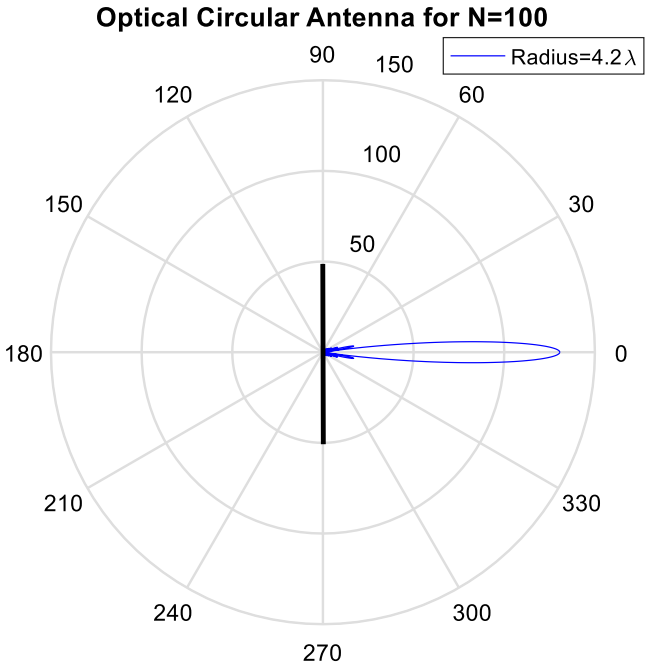

Figure 59 Radiation pattern of optical circular antenna radius of 4.2λ for N=100

Figure 58 shows on radius of 3.2λ for N=100. As seen Figure 58, the radiation field is contained in small beam which were primarily visible between the angles 30˚ to 330˚. Maximum radiation is the angle 0˚. Figure 59 shows on radius of 4.2λ for N=100. As seen Figure 59, the radiation field was contained in small beam which were primarily visible between the angles 30˚ to 330˚. Maximum radiation is the angle 0˚. As a result of these observations, when the radius increases, the radiation field has a narrower composition and radiation intensity is increased.

5.4 Radiation Pattern of Optical Quarter Circular Antenna

In this section observes on radiation pattern from Optical Quarter Circular Antenna (OQCA). The using the Eq. (4. 68) at radiation patterns different angles of circular (ϕ_0), observation angles ($\phi^{'}$) and constant segment of number (N) are determined in from OQCA. In the first analysis from OQCA, observation parameters are angle of circular $\phi_0 = 60$, observation angles $\phi^{'} = 30^0$, constant segment of $N = 100$ and

decreasing radius (a). Figure 60 shows on radius of 4.2λ and 3.2λ from $\phi_0 = 60$, $\phi' = 30^o$ and $N = 100$.

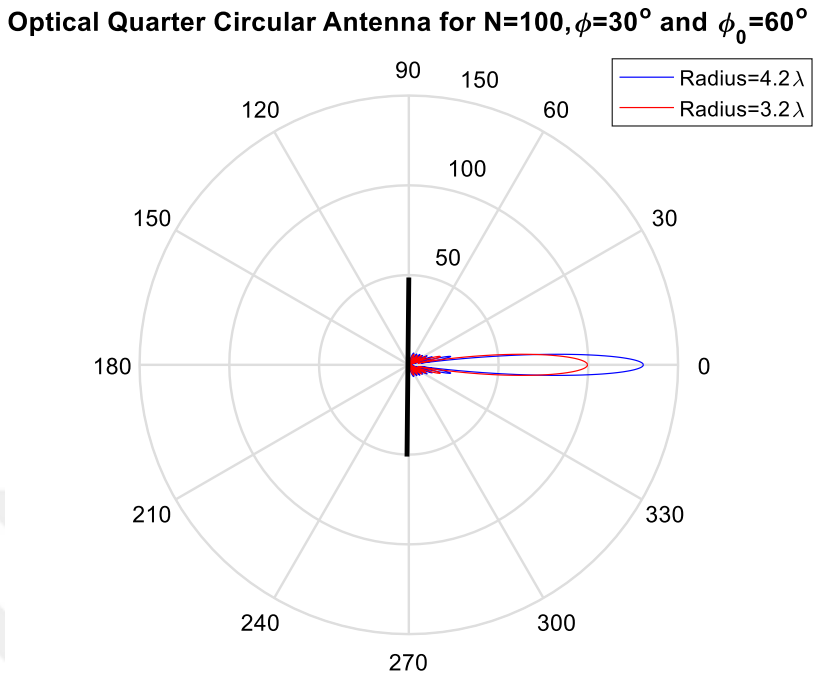

Figure 60 Radiation pattern of optical quarter circular antenna radius of 4.2λ and 3.2λ from $\phi_0 = 60$, $\phi' = 30^o$ and $N = 100$

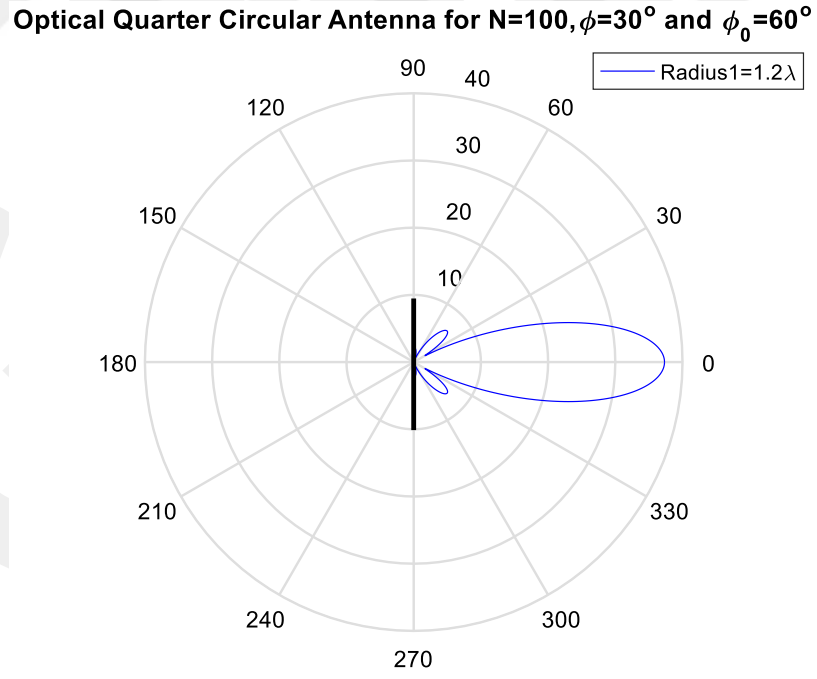

Figure 61 Radiation pattern of optical quarter circular antenna radius of 1.2λ from $\phi_0 = 60$, $\phi' = 30^o$ and $N = 100$

As seen in Figure 60, radiation pattern is observed on same direction and wide of beam but the coverage area of radius 3.2λ is smaller than the coverage area of radius 4.2λ. Figure 61 shows on radius of 1.2λ from $\phi_0 = 60$ and $\phi' = 30^o$. As seen in Figure 61, radiation pattern is observed on wide coverage area and low radiation density. Small beams are visible between the angles 60° to 330° from radius of 1.2λ. Maximum radiation is the angle 0° all of them. In the second analysis from OQCA observation parameters are angle of circular $\phi_0 = 60$, observation angles of $\phi' = 30^o$ and $\phi' = 90^o$, constant segment of $N = 100$ and radius of 1.2λ which shows on Figure 62. According to Figure 62, radiation pattern is observed same both of observation angles. The observations of $\phi' = 30^o$ and $\phi' = 90^o$ are inside and outside of antenna. The radiation field are the same the angles for $\phi' = 30^o$ and $\phi' = 90^o$. The size of the beams is different from each other.

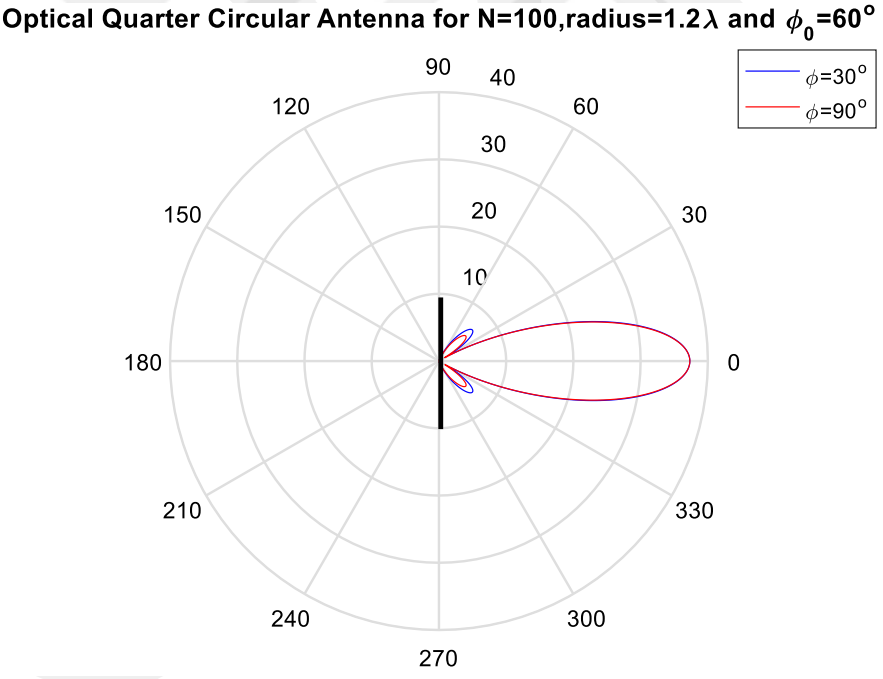

Figure 62 Radiation pattern of optical quarter circular antenna radius of 1.2λ from $\phi_0 = 60$, $\phi' = 30^o, \phi' = 90^o$ and $N = 100$

In the third analysis from OQCA, observation parameters are angle of circular $\phi_0 = 300$, observation angles $\phi' = 30^o$, constant segment of $N = 100$ and decreasing radius (a). Figure 63 shows on radius of 4.2λ and 3.2λ from $\phi_0 = 300$, $\phi' = 30^o$ and $N = 100$. As seen in Figure 63, radiation pattern is observed on same direction and wide of beam but the coverage area of radius 3.2λ is smaller than the coverage area of radius 4.2λ.

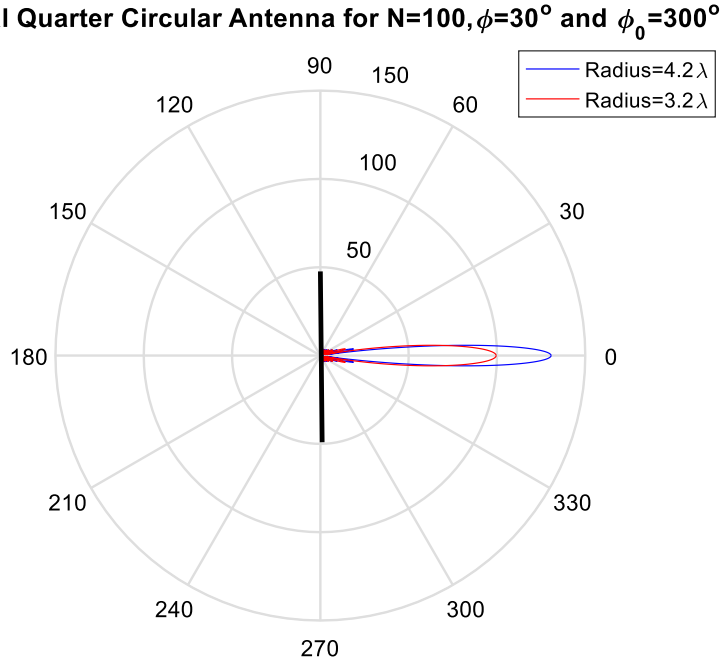

Figure 63 Radiation pattern of optical quarter circular antenna radius of 4.2λ and 3.2λ from $\phi_0 = 300$, $\phi' = 30^o$ and $N = 100$

Figure 64 shows on radius of 1.2λ from $\phi_0 = 300$, $\phi' = 30^o$ and $N = 100$. As seen in Figure 64, radiation pattern is observed on wide coverage area and low radiation density. Small beams are visible between the angles 60˚ to 330˚ from radius of 1.2λ. Maximum radiation is the angle 0˚ all of them. In the fourth analysis from OQCA observation parameters are angle of circular $\phi_0 = 300$, observation angles of $\phi' = 30^o$ and $\phi' = 330^o$, constant segment of $N = 100$ and radius of 1.2λ which shows on Figure 65. According to Figure 65, radiation pattern is observed same both of observation angles. The size of the beams is different from each other.

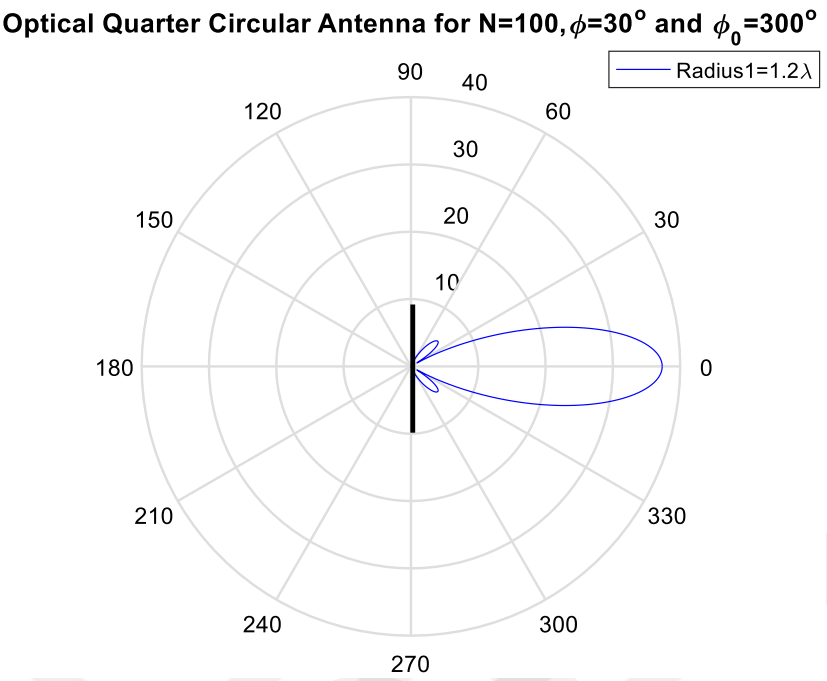

Figure 64 Radiation pattern of optical quarter circular antenna radius of 1.2λ from $\phi_0 = 300$, $\phi' = 30^o$ and $N = 100$

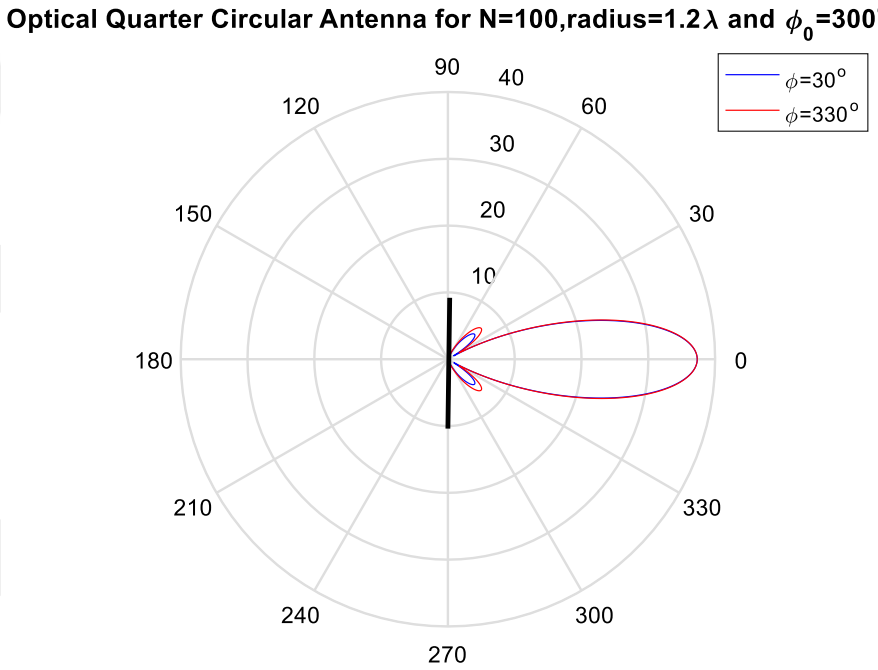

Figure 65 Radiation pattern of optical quarter circular antenna radius of 1.2λ from $\phi_0 = 300$, $\phi' = 30^o, \phi' = 330^o$ and $N = 100$

As a result of these observations, the radiation field is expanded when the radius of the OQCA is increased. Therefore, the radius of the OQCA increases the radiation field. Also, the same radiation field is observed on the inside and outside of the OQCA.

CHAPTER 6

CONCLUSION

In this thesis, the various design and the radiation patterns were investigated on the about optical antennas. These designs in the optical antennas were Optical Dipole Antenna, Optical Triangle Antenna, Optical Circular Antenna, and Optical Quarter Optical Antenna. The radiation patterns of these antennas have been calculated in the analytically with using integral of Physical Optics and were observed on them. The about thesis contents, contained in the six chapters. First chapter, in the literature were researched in about the optical antennas and the traditional antennas. Primarily, about the history of traditional antennas and specifications of optical antennas were mentioned. Then, in the works of literature were told in the properties of optical antennas. These the properties were contained in operation, techniques, the using materials, experimental setups and simulations in the optical antennas. The end of the chapter was told organization of this thesis. Second chapter, in the literature were researched in about fundamentals of light-matter interactions which were mentioned in the atomic models, the Photoelectric Effect, the energy bands of semiconductor. Researches about the atomic models were explained in. Applications of PE and the energy bands of semiconductor were given in about the information. Third chapter, operation, structure, production and application of the optical antennas were given in about the informations. The operation of optical antennas was mentioned on about interactions between electrons and photons. Behavior between electrons and photons were examined on the optical antennas. Structures of optical antenna were shown in and the production techniques of optical antenna were told. The end of the chapter, applications of optical antenna were told in about the studies in the literature. Fourth chapter, radiation pattern of optical antenna was calculated in the analytically with using integral of PO. These radiation patterns in the optical antennas were calculated

in for ODA, OTA, OCA, and OQCA. The radiation patterns in the ODA were observed in the different lengths, constant height and in the different heights, constant length for the angles of ϕ' and the segment of number N. The radiation patterns in the OTA were observed in the different lengths, constant height and in the different heights, constant length for the angles of ϕ' and the segment of number N. The radiation patterns in the OCA were observed in the different radius for the segment of number N. Fifth chapter, the radiation patterns in the OQCA were observed in the different radius for the angles of ϕ', the angles of circular (ϕ_0) and the segment of number N. Result of these observation were observed on radiation patterns different these parameters. These observations were told in the fifth chapter. Sixth chapter was conclusion.

As a result of this thesis, in these observations are available for every frequency and are observed that in these optical antennas changes in the length, the height, the radius, the angle that change radiation fields. In the literature, several researches have been done on the optical antennas, but these researches are experimental setups and simulations. In this thesis, the radiation fields are calculated analytically with using integral of PO. Therefore, Therefore, the thesis is an analytical solution with using integral of PO while working until this thesis.

REFERENCES

1. **Antenna Standards Committee of the IEEE Antennas and Propagation Society, (1993)**," *IEEE Standard Definitions of Terms for Antennas*", ISBN 1-55937-317-2.

2. **J. C. Maxwell, (1985)**, "*A Treatise on Electricity and Magnetism"*, Oxford University Press, London, UK, 1873, 1904.

3. **J. D. Kraus,** "*Antennas since Hertz and Marconi*", IEEE Trans. Antennas Propagat., Vol. AP-33, No. 2, pp. 131–137, February 1985.

4. **Sushruth Modak, (2014),**" *Frequency Selective Detection of Infrared Radiation in Uncooled Optical Nano-Antenna Array*", The degree of Master of Science in Optics in the College of Optics and Photonics at the University of Central Florida.

5. **Peter Mühlschlegel, (2006),**" *Optical Antennas*", The Degree of Doctor of Philosophy in the Faculty of Philosophy and Natural Sciences of the University of Basel.

6. **Giorgio Adamo, (2011),** "*Free-electron-driven nanoscale light sources: from Hertzian antennas to metamaterials*", The Degree of Doctor of Philosophy in the Faculty of Physical and Applied Science Optoelectronics Research Centre at the University of Southampton.

7. **Bharadwaj P., Deutsch B., Novotny L., (2009),** "*Optical Antennas*", Advances in Optics and Photonics 1, 438–483.

8. **Novotny L., (2007),** "The *History of Near-field Optics*", Progress in Optics 50, 137-184.

9. **E.H. Synge, (2009),**" *XXXVII. A suggested method for extending microscopic resolution into the ultra-microscopic region*", Philosophical Magazines 7, 356-362.

10. **Mario Agio, Andrea Alu, (2013)**," *Optical Antennas*", Cambridge University Press, ISBN 978-1-107-01414-5.

11. **Robert D. Grober, Robert J. Schoelkopf, Daniel E. Prober, (1997)**, "*Optical Antenna: Towards a Unity Efficiency Near-Field Optical Probe*", Appl. Phys. Lett. 70 (11), pp. 1354-1356.

12. **N. Pfullmann, C. Waltermann, M. Noack, S. Rausch, T. Nagy, C. Reinhardth, M. Kovacev, V. Knittel, R. Bratschitsch, D. Akemeier, A. Hutten, A. Leitenstorfer, U. Morger, (2013)**," *Bow-tie Nano-antenna Assisted Generation of Extreme Ultraviolet Radiation*", New Journal of Physics 15, 093027.

13. **Seungchul Kim, Jonghan Jin, Young-Jin Kim, In-Yong Park, Yunseok Kim, Seung-Woo Kim, (2008)**, "*High-harmonic Generation by Resonant Plasmon Field Enhancement*", Nature Letters, Vol. 453, p 757-760.

14. **Arvind Sundaramurthy, K. B. Crozier, G.S. Kino, D.P. Fromm, P.J. Schuck, W.E. Moerner, (2005)**, "*Field Enhancement and Gap-dependent Resonance in a System of Two Opposing tip-to-tip Au Nanotriangles*", Physical Review B, Vol. 72, pp. 165409-1 – 165409-6.

15. **P. James Schunk, David P. Fromm, W.E Moerner, Arvind Sundaramurthy, Gordon Kino**, **(2005)**," *Gold Bowtie Nanoantennas: Improving the Mismatch between Light and Nanoscale Objects*", OSA.

16. **K.B. Crozer, A. Sundaramurthy, G.S. Kino, C.F. Quate, (2003)**," *Optical Antennas: Resonators for Local Field Enhancement*", Journal of Applied Physics, Vol. 95, No. 7, pp. 4632- 4642.

17. **David P. Fromm, Arvind Sundaramurthy, P. James Schuck, Gordon Kino, W.E. Moerner**, **(2004)**," *Gap-Dependent Optical Coupling of Single "Bowtie" Nanoantennas Resonant in the Visible*", Vol.4, No.5, pp. 957-961.

18. **Christophe Fumeax, Javier Alda, Glenn D. Boreman, (1999)**, "*Lithographic Antennas at Visible Frequencies*", Optics Letters, Vol. 24, No.22, pp.1629-1631.

19. **D. Bala Sekhar, Avanish Bhadauria, William R. Taube, (2013)**," *Parameter Dependency of Dipole Nanoantenna in Infrared Range*", META'13 Conference, 18-22 March 2013, Sharjah – United Arab Emirates.

20. **Liang Tang, Sukru Elkin Kocabas, Salman Latif, Ali K. Okyay, Dany-Sebastian LY-Gangnon, Krishna C. Saraswat, David A.B. Miller, (2008)**," *Nanometer-Scale Germanium Photodetector Enhanced by a Near-Infrared Dipole Antenna*", Nature Photonics.

21. **N. Cazier, M. Buret, A. V. Uskov, L. Markey, J. Arocas, G. Colas, Des Francs, A. Bouhelier, (2016)**," *Electrical excitation of waveguided surface plasmons by a light-emitting tunneling optical gap antenna*", Optic Express, Vol. 24, No. 4, pp. 3873-3884

22. **Kosei Ueno, Quan Sun, Mashiro Mino, Takumi Itoh, Tomoya Oshikiri, Hiroaki Misawa, (2016)**," *Surface plasmon optical antennae in the infrared region with high resonant efficiency and frequency selectivity*", Optic Express, Vol. 24, No. 16, pp. 17728-17737

23. **Jongbum Kim, Aveek Dutta, Gururaj V. Naik, Alexander J. Giles, Francisco J. Bezares, Chase T. Ellis, Joseph G. Tischler, Ahmed M. Mahmoud, Humeyra Caglayan, Orest J. Glembocki, Alexander V. Kildishev, Joshua D. Caldwell, Alexandra Boltasseva, Nader Engheta, (2016)**," *Role of epsilon-near-zero substrates in the optical response of plasmonic antennas*", Optical Society of America, Vol. 3, No. 3, pp. 339-346

24. **Vahid Khoshdel, Mehrdad Shokooh-Saremi, (2017)**," *Design and optimization of slot nano-antennas for ambient thermal energy harvesting*", Optics, Vol.138, pp. 470-475

25. **Rachakonda A.N.S. Aditya, Anand Sreekantan Thampy, (2018)**," *Field enhanced graphene based dual hexagonal ring optical antenna for tip-enhanced spectroscopy*", Infrared Physics & Technology, Vol. 90, pp. 70-77

26. **Rodney LOUDON, (2000)**," The *Quantum Theory of Light Third Edition*", Department of Electronic Systems Engineering University of Essex, ISBN 0 19 850176 5.

27. **K.Y. Bliokh, F.J. Rodrígez-Fortuño, F. Nori, A.V. Zayats, (2015)**, "Spin-*orbit interaction of light*", Nature Photonics, Vol. 9, pp. 796-808.

28. **David Harvey, (2000)**," *Modern Analytic Chemistry*", John Wiley & Sons, ISBN 0-07-237547-7.

29. **J.J. Thomson**, **(1897)**, "*Cathode Rays*", Philosophical Magazine, Vol. 44, No. 293, pp. 1897- 1921.

30. **Robert EISBERG, Robert RESNICK**, **(1985)**," *QUANTUM PHYSICS of Atoms, Molecules, Solids, Nuclei, and Particles Second Edition*", John Wiley & Sons, ISBN 0-471-87373-X.

31. **E. Rutherford, (1911)**, "*The Scattering of α and β Particles by Matter and the Structure of the Atom*", Philosophical Magazine, Series 6, Vol. 21, pp. 669-688.

32. **N. Bohr, (1913)**," *On the Constitution of Atoms and Molecules*", Philosophical Magazine, Vol. 26, No. 1 pp. 1913-1937.

33. **N. Bohr, (1913)**," *On the Constitution of Atoms and Molecules – Part II. – Systems Containing only a Single Nucleus*", Philosophical Magazine, Vol. 26, No. 476 pp. 1913-1939.

34. **N. Bohr**, **(1913)**," *On the Constitution of Atoms and Molecules – Part III. – Systems Containing Several Nucleus*", Philosophical Magazine, pp.857-875.

35. **Stephen Gasiorowiez**, **(2003)**, "*Quantum Physics Third Edition*", John Wiley & Sons, ISBN 0-471-42945-7.

36. **M. Planck**, **(1901)**," *Ueber das Gesetz der Energieverteilung im Normalspektrum*", Annalen der Physik, Vol. 309, No. 3, pp. 553-563.

37. **M. Planck**, **(1905)**," *Über einen die Erzeugung und Verwandlung des Lichtes betreffend heuristischen Gesichtspunkten*", Annalen der Physik, Vol. 322, No. 6, pp. 132-148.

38. **Charles Kittel**, **(2005)**, "*Introduction to Solid State Physics Eight Edition*", John Wiley & Sons, ISBN 0-471-68057-5.

39. **Hebert B. Michaelson, (1977)**, "*The work function of the elements and its periodicity*", Journal of Applied Physics, Vol. 48, No. 11, pp. 4729-4733.

40. **V. I. Klimov, A. A. Mikhailovsky, Su Xu, A. Malko, J. A. Hollingsworth, C. A. Leatherdale, H.-J. Eisler, M. G. Banwedi, (2000)**," *Optical Gain and Stimulated Emission in Nanocrystal Quantum Dots*", Science, Vol. 290, pp. 314-317.

41. **V. L. Colvin, M. C. Schlamp, A. P. Alivisatos, (1994)**," *Light-emitting diodes made from cadmium selenide nanocrystals and a semiconducting polymer*", Nature Publishing Group, Vol. 370, pp. 354-357.

42. **N. C. Greenham, Xiaogang Peng, A. P. Alivisatos, (1996)**, "*Charge separation and transport in conjugated polymer semiconductor nanocrystal composites studied by photoluminescence quenching and photoconductivity*", Physical Review B, Vol. 54, No. 24 pp. 17628-17637

43. **Yongqi Liang, Lin Zhai, Xinsheng Zhao, Dongsheng Xu, (2005)**," Band-*Gap Engineering of Semiconductor Nanowires through Composition Modulation*", The Journal of Physical Chemistry B, Vol. 109, No. 15, pp. 7120-7123

44. **Bahaa E. A. Saleh, Malvin Carl Teich (1991),** "*Fundamentals of Photonics*", John Wiley& Sons Inc., ISBN 0-471-83965-5

45. **Lukas Novonty, Niek van Hulst**, **(2011)**," *Antennas for light*", Nature Photonics, Vol. 5, pp.83-90.

46. **R. Esteban, T.V. Teperik, J.J. Grefet**, **(2010)***," Optical Patch Antennas for Single Photon Emission Using Surface Plasmon Resonances*", Physical Review Letters, American Physical Society, Vol. 104, pp. 026802.

47. **Jung-Hwan Song, Jonghwa Shin, Hee-Jin Lim, Yong-Hee Lee**, **(2011)**," *Optical recoil of asymmetric nano-optical antenna*", Optical Society of America, Vol. 19, No. 16, pp. 14929 – 14936.

48. **S. Mokkapati, D. Saxena, H. H. Tan, C. Jagadish**, **(2015)**, "*Optical design of nanowire absorbers for wavelength selective photodetectors*", Scientific Reports, Vol.5, No. 15339, pp. 1-7.

49. **Tae Joon Seok, Arash Jamshidi, Myungki Kim, Scott Dhuey, Amit Lakhani, Hyuck Choo, Peter James Schuck, Stefano Cabrini, Adam M. Schwartzberg, Jeffrey Bokor, Eli Yablonovitch, Ming C. Wu**, **(2011)**, "*Radiation Engineering of Optical Antennas for Maximum Field Enhancement*", Nano Letters, Vol. 11, No.7, pp. 2606-2610.

50. **Tun Cao, Chen-wei Wei, Robert E. Simpson, Lei Zhang, Martin J. Cryan**, **(2014)**," *Broadband Polarization-Independent Perfect Absorber Using a Phase-Change Metamaterial at Visible Frequencies*", Scientific Reports, Vol.5, No. 3955, pp. 1-8.

51. **G. S. Unal, M. I. Aksun**, **(2015)**," *Bridging the Gap between RF and Optical Patch Antenna Analysis via the Cavity Model*", Scientific Reports, Vol.5, No. 15941, pp. 1-8.

52. **Bublu Mukherjee, Asim Guchhait, Yinthai Chan, Ergun Sımsek**, (2015)," *Absorptance of PbS Quantum Dots Thin Film Deposited on Trilayer MoS_2*", Advance Matter Letters, Vol. 6, No. 11, pp. 936-940.

53. **Peter Mühlshlegel**, **(2006)**," *Optical Antennas*", The Degree of Doctor of Philosophy in the Faculty of Philosophy and Natural Sciences of the University of Basel.

54. **Hans-Georg Braun**, **(2008)**, "*Electron beam lithography*", M.A. McCord, Stanford University and M.J. Rocks, Cornell University.

55. **P. Mühlshlegel, H-J. Eisler, O. J. F. Martin, B. Hetch, D. W. Pohl, (2005)**," *Resonant optical antennas*", Science, Vol. 308, No. 5728, pp. 1607-1609.

56. **T. Hanke, G. Krauss, D. Trautlein, B. Wild, R. Bratschitsch, A. Leitenstrofer, (2009),** "*Efficient Nonlinear Light Emission of Single Gold Optical Antennas Driven by Few-Cycle Near Infrared Pulses*", Physical Review Letters, vol. 130, pp. 257404-1-257404-4.

57. **Linyou Cao, Joon-Shink Park, Pengyu Fan, Bruce Clemens, Mark L. Brongersma, (2010)**," *Resonant Germanium nanoantenna photodetectors*", Nano Letters, Vol. 10, No. 4, pp. 1229-1233.

58. **Ertugrul Cubukcu, Eric A. Kort, Kenneth B. Crozier, Federico Capasso, (2006)**," *Plasmonic laser antenna*", Applied Physics Letters, Vol. 89, No. 9, pp. 093120-1-093120-3.

59. **S. Pilla, K. R. Catchpole, T. Trupke, M. A. Green, (2007)**, "*Surface plasmon enhanced silicon solar cells*", Journal of Applied Physics, Vol. 101, No. 9, pp. 093105-1-093105-8.

60. **Jeffrey N. Anker, W. Paige Hall, Olga Lyanders, Nilam C. Shah, Jing Zhao, Richard P. Van Duyne, (2008)**," *Biosensing with plasmonic nanosensors*", Nature Materials, Vol. 7, pp. 442-453.

61. **Jon A. Schuller, Thomas Taubner, Mark L. Brongersma, (2009)**," *Optical antenna thermal emitters*", Nature Photonics, Vol. 3, pp. 658-661.

62. **Yannick De Wilde, Florian Formanek, Remi Carminati, Boris Gralak, Paul-Arthur Lemoine, Karl Joulain, Jean-Philippe Mulet, Yong Chen, Jean-Jacques Greffet, (2006)**," *Thermal radiation scanning tunnelling microscopy*", Nature Letters, Vol. 444, pp. 740-743.

63. **Lukas Novonty, Stephen J. Stranick, (2006)**," *Near-field optical microscopy and spectroscopy with pointed probes*", Annual Review of Physical Chemistry, Vol. 57, pp. 303-331.

64. **U. Ch. Fischer, D. W. Pohl, (1989)**," *Observation of Single-Particle Plasmons by Near-Field Optical Microscopy*", Physical Review Letters, Vol. 62, No. 4, pp. 458-461.

65. **McDonald H. M., (1913)**, "*The Effect Produced by An Obstacle on A Train of Electric Waves*", Phil. Trans. R. Soc. Lond., Ser. A., Math. Phys. Sc., vol. 212, pp. 299-337.

66. **Warren L. Stutzman, Gary A. Thiele, (2013),** "*Antenna Theory and Design Third Edition*", John Wiley& Sons Inc., ISBN 978-0-470-57664-9.

APPENDICES A

CURRICULUM VITAE

PERSONAL INFORMATION

Surname, Name: DÜNDAR, Ulvihan Uğur

Date and Place of Birth: 21 August 1986, Samsun

Marital Status: Single

Phone: +90 505 603 66 57

Email: uuurdundar@gmail.com

EDUCATION

Degree	Institution	Year of Graduation
M.Sc.	Çankaya Univ., Occupational Health and Safety	2016
B.Sc.	Çankaya Univ., Elec. And Comm. Engineering	2013
Associate Degree	Ankara Univ. Kalecik Vocational School, Landscape	2007
High School	Kalaba High School	2003

WORK EXPERIENCE

Year	Place	Enrollment
2018 – Present	Rakun Bilişim ve Arge Teknolojileri	Project Engineer
2015 – 2018	GO Enerji A.Ş.	Field Engineer
2014 - 2015	Antensan Haberleşme Hüsnü Deniz BAŞDEMİR	R&D Engineer

2012 June	Telesis Telekomünikasyon Sistemleri	Trainier
2011 August	Türk Havacılık ve Uzay Sanayi A.Ş. (TUSAŞ- TAI)	Trainier

FOREIN LANGUAGES
Advanced English, Beginner Spanish

PUBLICATIONS

1. Ulvihan Uğur DÜNDAR, Yrd. Doç. Dr. Mustafa Alp ERTEM, (2017), "*Güneş Enerjisi Santralleri Kurulumu İçin Risk Değerlendirme Rehberi*", IX. Ulusal İşçi Sağlığı ve İş Güvenliği Kongresi ve Sergisi, (31.11.2017-02.12.2017).

HOBBIES
Swimming, Chess, Photography